J. COMBIN. MATH. COMBIN. COMPUT. 127a (2025) 5399--5434

Journal of Combinatorial Mathematics and Combinatorial Computing
www.combinatorialpress.com/jcmcc

Efficient numerical simulation and method optimization for pressure distribution calculation in petroleum seepage field

Yisen Wang[1,✉], Hongwei Wang[2], Feng Bian[3]

[1] *Southwest Petroleum University, Chengdu, Sichuan, 610000, China*

[2] *Development and Planning Department, Dagang Oilfield Company, Tianjin, 300280, China*

[3] *No.4 Oil Production Plant, Dagang Oilfield Company, Tianjin, 300280, China*

ABSTRACT

In this paper, a pressure distribution model of seepage field based on complex reservoir conditions is established based on a finite element mathematical model. Due to the non-homogeneity and multiple flow characteristics of the reservoir, the mathematical model of fractured horizontal wells based on reservoir and fracture is established by solving the finite element equations of oil-phase pressure and water-phase saturation under the two-dimensional oil-water two-phase finite element model. Through numerical simulation of the coupling between the permeability change of the fractured fracture and the bedrock in the oil seepage field, the influence of different fracture parameters on the pressure distribution is analyzed, and each parameter is optimized. Investigations of stress-strain, porosity and permeability in time and space in low-permeability reservoirs found that in the region near the bottom of the well, each parameter varies more, while the farther away from the bottom of the well region the less affected it is. The relative position of the fracture to the well has a large effect on the production of fractured horizontal wells, but this parameter can be artificially regulated. Repeated fracturing cumulative oil incremental analysis found that "fracture network bandwidth, main fracture half-length and main fracture inflow capacity" have the greatest influence on the high permeability strip, the factors of angular wells and low permeability zones, and the repeated fracturing cumulative oil incremental simulation of each fracture parameter has the greatest effect on the fracture network bandwidth, main fracture half-length and main fracture inflow capacity under the coupled model of Well 3 (23.25%), and the optimal values of the parameters are 100m, 100m, 100m, 100m, 100m, 100m and 100m respectively. optimal values of the parameters are 100 m, $150\times10^{-3}\mu m^2\cdot m$, 20 m and $45\times10^{-3}\mu m^2\cdot m$, respectively.

Keywords: finite element mathematical model; seepage field pressure distribution model; fractured horizontal well mathematical model; oil seepage field

1. Introduction

With the improvement of China's petroleum exploration and development, the proportion of low

✉ Corresponding author.
E-mail address: 18920986272@163.com (Y. Wang).

Received 20 February 2024; Revised 15 May 2024; Accepted 20 November 2024; Published Online 15 April 2025.
DOI: 10.61091/jcmcc127a-303

permeability oil field reserves is getting bigger and bigger, and the proportion of low permeability reserves in the proven unused petroleum geological reserves is as high as more than one, and it is on a rising trend year by year. In the face of China's major oil fields have entered the middle and late stage of development, in the current situation of tight oil reserves, how to utilize and develop low permeability oil fields, improve the efficiency of exploitation, the sustainable and stable development of China's petroleum industry is of great practical significance [1-3].

Although China's low-permeability reservoirs have great resource potential, the natural production capacity of the wells is very low due to their low permeability, high seepage resistance, and poor connectivity, which cannot meet the demand of economic development [4-5]. Therefore, in order to increase the production of a single well and improve the development effect, the development technology of low permeability reservoirs needs to be effectively modified. Currently, horizontal well fracturing technology is used as the main means to develop low-permeability reservoirs, expanding the drainage area of a single well by means of pressing multiple fractures into the horizontal wells, thus increasing the production capacity of the horizontal wells and improving the development effect of low-permeability oil fields [6-9]. To extract coal gas or oil by horizontal wells, engineering attaches great importance to the pressure distribution of fluids near the wellbore of horizontal wells, which is related to the ability to reasonably determine the production rate of oil and gas wells, so as to ensure the stable and long-term exploitation of oil and gas wells [10-12]. Therefore, when a horizontal well is used to extract coal gas or oil, the accurate calculation of the pressure distribution of the fluid seepage field in its horizontal wellbore becomes very important [13-14]. And due to the inhomogeneity of reservoir rocks and the complexity of pore structure, what occurs within the reservoir is often a non-uniform flow of fluids, especially when encountering horizontal wells with long horizontal sections, there is a possibility of encountering a variety of complex reservoir geologic bodies [15-18]. In order to successfully implement the horizontal well fracturing modification, it is necessary to conduct an in-depth study on the influence law of fracture parameters as well as well network parameters on the production capacity of fractured horizontal wells, and optimize each parameter to ensure the production capacity of the fractured horizontal wells [19-21].

Since the emergence of horizontal wells, many researchers have paid great attention to the seepage problem in this reservoir and have done a lot of work. Literature [22] studied the stress produced by fluid seepage on the rock around the wellbore, and established a borehole collapse pressure model based on seepage mechanics and linear elasticity theory, which is conducive to reducing the risk of underbalanced drilling in horizontal wells. Literature [23] established a pore pressure distribution model under anisotropic seepage conditions in horizontal wells based on seepage effect and thermal effect in underbalanced drilling, which can obtain more accurate results of horizontal underpressure wells and provide stability analysis for the safety and security of the wellbore. Literature [24] designs a transient calculation model of single-phase flow in horizontal wells from the perspective of reservoir seepage and horizontal wellbore flow, which can optimize the oil and gas production work based on massive data. Literature [25] proposed a mathematical model describing multi-fractured horizontal wells in rectangular outer boundary reservoirs, which can analyze and evaluate the production dynamics of reservoir wells in order to guarantee the low-risk and high-production performance of the wells. Literature [26] shows that the induced stress generated by multiple wells affects the formation of complex fractures in horizontal wells, and uses linear superposition and vector representation to establish a production capacity model of the horizontal stress field between wells, which provides a theoretical basis for the optimal spacing of wells and the formulation of fracturing programs for the reservoir extraction process by analyzing the changing law of the induced stress field in the cluster of horizontal wells. Literature [27] established a computational model of oil and gas two-phase flow instability in horizontal wells, which effectively simplified the seepage model of horizontal well extraction reservoirs, and only simulated the calculation of wells without considering the complex grid division, which improved the simulation speed of the reservoir model. It can be seen that most of the studies have made many simplifications of the model, and often only for a particular reservoir type, the simplified model can only solve the seepage problems of some specific homogeneous reservoir types, which can not solve the actual seepage problems of various complex factors analytical methods, so to solve the seepage problems of the reservoirs of the complex geologic bodies containing horizontal wells, numerical methods is not a better choice.

In this paper, on the basis of the basic principle of finite element method, combined with the seepage characteristics of low-permeability reservoirs, differential equations of oil-water two-phase seepage, finite element equations of oil-phase pressure and finite element equations of water-phase saturation are modeled, and a finite element mathematical model of oil seepage field is established. On the basis of the Warren-Root model, an unstable seepage model of fractured horizontal wells in extra-low-permeability reservoirs under consideration of the initiating pressure gradient is established. Using the basic seepage mechanics theory such as pressure drop superposition principle and line source function, Laplace transform and Stehfest numerical inversion are applied to calculate and determine the pressure distribution of fractured horizontal wells, which can be converted to the actual space by the numerical inversion method, and then solved by using Stehfest numerical inversion. Finally, the influence of natural fracture parameters on yield and pressure in the seepage model of fractured non-homogeneous composite reservoirs is explored as well as the optimization of fracture parameters for repeated modification of volumetric fracturing.

2. Efficient numerical simulation methods for calculating pressure distributions in oil seepage fields

2.1. Finite element fundamentals

2.1.1. Equivalent Integral Forms and Weighted Residual Methods:

1) Equivalent integral form of differential equations. Within practical engineering and physics, problems are usually formulated in the form of differential equations and boundary conditions satisfied by the unknown field function, which u should satisfy the set of differential equations:

$$A(u)=\begin{pmatrix} A_1(u) \\ A_2(u) \\ \vdots \end{pmatrix}=0\left(In\,\Omega\right) \tag{1}$$

The solution region and boundary are shown in Figure 1. The domain Ω can be a volume domain, an area domain, etc., while the unknown function u should also satisfy the boundary conditions:

$$B(u)=\begin{pmatrix} B_1(u) \\ B_2(u) \\ \vdots \end{pmatrix}=0\left(On\,\Gamma\right) \tag{2}$$

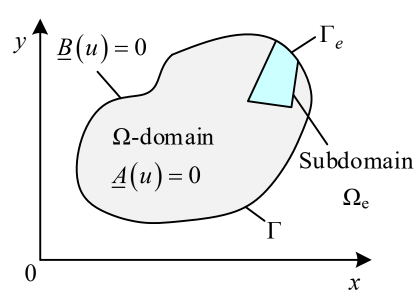

Fig. 1. Solve the area Ω and the boundary Γ

In the figure A, B denote the differential operators of independent variables. As an example, the mathematical modeling of the heat conduction equation in the two-dimensional steady state is established to solve the control equations and the boundary fixed solution conditions as follows:

$$A(\varphi)=\frac{\partial}{\partial x}\left(k\frac{\partial\varphi}{\partial x}\right)+\frac{\partial}{\partial y}\left(k\frac{\partial\varphi}{\partial y}\right)+q=0\ \left(In\ \Omega\right) \tag{3}$$

$$B(\phi)=\begin{cases}\phi-\overline{\phi}=0 & \left(On\ \Gamma_{\phi}\right)\\ k\dfrac{\partial\phi}{\partial n}-\overline{q}=0 & \left(On\ \Gamma_{q}\right)\end{cases} \tag{4}$$

In the equations φ denotes the temperature; k is the fluidity or heat transfer coefficient; $\overline{\phi}$ and $\overline{q}$ are given values of temperature and heat flow on the boundary; n is the direction of the outer normal to the boundary Γ in question; and q is the source density.

Since the set of differential equations (1) must be zero at every point in the domain Ω, it is obtained:

$$\int_{\Omega}V^{T}A(u)d\Omega\equiv\int_{\Omega}\left(v_1A_1(u)+v_2A_2(u)+\cdots\right)d\Omega\equiv 0 \tag{5}$$

In the formula:

$$V=\begin{pmatrix}v_1\\ v_2\\ \vdots\end{pmatrix} \tag{6}$$

where V represents a vector of functions, and the number of arbitrary functions in the set is equal to the number of differential equations.

Similarly, if the boundary condition (2) can also be satisfied at every point on the boundary at the same time, the following equation should hold for a set of arbitrary function vectors $\overline{V}$:

$$\int_{\Gamma}\overline{V}^{T}B(u)d\Gamma\equiv\int_{\Gamma}\left(\overline{v}_1B_1(u)+\overline{v}_2B_2(u)+\cdots\right)d\Gamma\equiv 0 \tag{7}$$

Then the equivalent integral form of the differential equation is finally obtained:

$$\int_{\Omega}V^{T}A(u)d\Omega+\int_{\Gamma}\overline{V}^{T}B(u)d\Gamma=0 \tag{8}$$

2) The "weak" form of the equivalent integral. Another form of the differential equation is obtained by partial integration of equation (8):

$$\int_{\Omega}C^{T}(v)D(u)d\Omega+\int_{\Gamma}E^{T}(\overline{v})F(u)d\Gamma=0 \tag{9}$$

The C, D, E, and F in the above equation are differential operators, and the order of the derivatives in these operators is lower than the order of A in equation (8), so it is sufficient to demand only the continuity of the function u to its lower order.

Weighted residual method

In the physical problem expressed by the differential equation (1) equation and the boundary condition (2) equation, an approximation function can be used to represent the unknown field function u. Namely:

$$u\approx\overline{u}=\sum_{i=1}^{n}N_ia_i=Na \tag{10}$$

where a_i is the parameter to be determined in Eq. N_i is the form function, which is known, taken from a complete sequence of functions, and is linearly independent. For example when the unknown function u represents the pressure, its approximate solution can be taken as:

$$u = N_1 u_1 + N_2 u_2 + \cdots + N_n u_n = \sum_{i=1}^{n} N_i u_i \tag{11}$$

At finite values of n, the approximate solution does not satisfy exactly the differential equation (1) equation and the boundary conditions (2), and they will produce residuals R and $\overline{R}$:

$$A(Na) = R; B(Na) = \overline{R} \tag{12}$$

The residuals R and $\overline{R}$ are also called residuals. In equation (8) we replace the arbitrary functions v and $\overline{v}$ by n approximate functions, where $u = N_1 u_1 + N_2 u_2 + \cdots + N_n u_n = \sum_{i=1}^{n} N_i u_i$ is the n approximate function.

The approximate equivalent integral form of the original differential equation is obtained:

$$\int_\Omega W_j A(Na) d\Omega + \int_\Gamma \overline{W}_j^T B(Na) d\Gamma = 0 (j = 1 \sim n) \tag{13}$$

The remaining quantities can be written in the form:

$$\int_\Omega W_j^T R d\Omega + \int_\Gamma \overline{W}_j^T \overline{R} d\Gamma = 0 (j = 1 \sim n) \tag{14}$$

Eqs. W_j and $\overline{W}_j$ are called weight functions. A set of equations can be obtained under the condition that the weighted integral of the residual is zero, and by solving the equations the coefficients to be determined for the approximate solution a_i can be determined to obtain an approximate solution to the original problem. Equation (13) is expanded in the form:

$$\begin{gathered}
\int_\Omega W_1^T A(Na) d\Omega + \int_\Gamma \overline{W}_1^T B(Na) d\Gamma = 0 \\
\int_\Omega W_2^T A(Na) d\Omega + \int_\Gamma \overline{W}_2^T B(Na) d\Gamma = 0 \\
\cdots\cdots\cdots \\
\int_\Omega W_n^T A(Na) d\Omega + \int_\Gamma \overline{W}_n^T B(Na) d\Gamma = 0
\end{gathered} \tag{15}$$

Assuming that the number of differential equations A is m_1 and the number of boundary conditions B is m_2, the weight function $W_j (j = 1, \ldots, n)$ is a functional array of order m_1 and $\overline{W}_j (j = 1, \cdots, n)$ is a functional array of order m_2.

Similarly, the equivalent integral "weak" form of the differential equation is approximated by:

$$\int_\Omega C^T \left(W_j\right) D(Na) d\Omega + \int_\Gamma E^T \overline{W}_j F(Na) d\Gamma = 0 (j = 1, \cdots, n) \tag{16}$$

The weighted residual method can be widely used for various types of equations, and different weighted residual methods can be produced by choosing different weight functions.Galerkin's method has a wide range of applicability, and its basic principle is:

Take $W_j = N_j$ and $\overline{W}_j = -W_j = -N_j$ on the boundary, i.e., choose the sequence of form functions that approximate the solution as the weight function. Then its approximate integral form is:

$$\begin{gathered}
\int_\Omega N_j^T A\left(\sum_{i=1}^{n} N_i a_i\right) d\Omega - \int_\Gamma N_j^T B\left(\sum_{i=1}^{n} N_i a_i\right) \\
d\Gamma = 0 (j = 1, 2, \cdots, n)
\end{gathered} \tag{17}$$

Define the variant $\delta\tilde{u}$ of the approximate solution $\tilde{u}$ as:

$$\delta\tilde{u} = N_1 \delta a_1 + N_2 \delta a_2 + \cdots + N_n \delta a_n \tag{18}$$

Then, the above equation can be organized as:

$$\int_\Omega \delta\tilde{u}^T A(\tilde{u}) d\Omega - \int_\Gamma \delta\tilde{u}^T B(\tilde{u}) d\Gamma = 0 \tag{19}$$

Similarly, an approximate form for the "weak" form of the equivalent integral can be obtained:

$$\int_{\Omega} C^T(\delta\tilde{u})D(\tilde{u})d\Omega + \int_{\Gamma} E^T(\delta\tilde{u})F(\tilde{u})d\Gamma = 0 \tag{20}$$

2.1.2. Variational principle. The discussion of the "variational principle" [28] for a continuous medium problem begins with the creation of a scalar generalized function Π, which has the integral form:

$$\Pi = \int_{\Omega} F\left(u, \frac{\partial u}{\partial x}, \cdots\right) d\Omega + \int_{\Gamma} E\left(u, \frac{\partial u}{\partial x}, \cdots\right) d\Gamma \tag{21}$$

where u is the unknown function, F and E are specific operators, Ω is the solution domain, and Γ is the boundary of the solution domain Ω. The generalized function of the unknown function u is that Π varies as the unknown function u varies. The solution u of the continuous medium problem is such that the generalized function Π takes standing values for small changes δu in:

$$\delta\Pi = 0 \tag{22}$$

This method of solving the solution of a continuous medium problem is called variational principle or variational method.

2.1.3. General Steps in Finite Element Methods. The finite element method always solves the general continuous medium problem step by step in a sequential manner. The finite element method always solves the general continuous medium problem in a step-by-step manner. The basic steps of the finite element method are:

1) Discretization of the structure. The specific practice of discretization is to discretize a continuous solution domain into a certain number of finite number of small unit aggregates, and the units are only interconnected at the nodes.
2) Selection of interpolation function. Under the action of any given constraint, the exact solution of the problem is unknown, so we approximate the unknown exact solution with the appropriate solution within the cell. The chosen interpolation function must guarantee the convergence of the finite element solution, and the interpolation function of the solution is usually written in polynomial form.
3) Unit analysis. Use the equilibrium conditions or variational principle to establish the unit stiffness matrix Ke and load vector Fe of unit e, and obtain the unit balance equation.
4) Compose the total stiffness matrix to establish the equilibrium equation of the structure. Assemble the stiffness matrix and load vector separately to obtain the overall balance equation of the structure.
5) Introduce constraints. Modify the overall balance equation of the structure according to the boundary conditions of the problem.
6) The equations are solved and other parameters are calculated.

2.2. Finite element mathematical modeling of oil seepage field

2.2.1. Differential equations for oil-water two-phase seepage flow. Basic assumptions:

1) There is an oil-water two-phase fluid in the reservoir;
2) The reservoir is non-homogeneous and anisotropic;
3) Both the fluid and the rock are slightly compressible;
4) Consider the effect of capillary forces;
5) Neglect the effect of gravity;
6) The model is two-dimensional.

The differential equation for oil-water two-phase seepage is:

$$\nabla\left(\rho_o \frac{K \cdot K_{ro}}{\mu_o} \nabla p_o\right) + q_o = \frac{\partial\left(\phi S_o \rho_o\right)}{\partial t} \tag{23}$$

$$\nabla\left(\rho_w \frac{K \cdot K_{rw}}{\mu_w} \nabla p_w\right) + q_w = \frac{\partial\left(\phi S_w \rho_w\right)}{\partial t} \tag{24}$$

Where equation (23) is the oil phase equation and equation (24) is the water phase equation. The auxiliary equations are:

$$\rho_o = \rho_o\left(p_o\right) \tag{25}$$

$$\rho_w = \rho_w\left(p_w\right) \tag{26}$$

$$K_{ro} = K_{ro}\left(S_o\right) \tag{27}$$

$$K_{rv} = K_{rw}\left(S_w\right) \tag{28}$$

$$\phi = \phi\left(p_o\right) \tag{29}$$

$$p_c = p_c\left(S_w\right) = p_o - p_w \tag{30}$$

$$S_o + S_w = 1 \tag{31}$$

Initial conditions are:

$$\begin{aligned} p_o\big|_{(t=0)} &= p_{ot} \\ S_w\big|_{t=0} &= S_{wi} \end{aligned} \tag{32}$$

The outer boundary conditions are:

$$\begin{aligned} \left.\frac{\partial p_o}{\partial n}\right|_{\Gamma 1} &= 0 \\ p\big|_{\Gamma 2} &= p_{con} \\ \left.\frac{\partial s_w}{\partial n}\right|_{\Gamma 3} &= 0 \end{aligned} \tag{33}$$

The inner boundary conditions are:

$$\lambda \left.\frac{\partial P_o}{\partial n}\right|_{\Gamma 4} = \frac{2\pi K h}{\mu \ln \frac{r}{r_w}}\left(p - p_{wf}\right) \tag{34}$$

$$\left.\frac{\partial P_o}{\partial n}\right|_{\Gamma 5} = q \tag{35}$$

$$S_w = S_{w0} \tag{36}$$

Let the flow coefficients $\lambda_{wx} = \frac{K_x K_{rw}}{\mu_w}$; $\lambda_{wy} = \frac{K_y K_{rw}}{\mu_w}$; $\lambda_{ox} = \frac{K_x K_{ro}}{\mu_o}$; $\lambda_{oy} = \frac{K_y K_{r0}}{\mu_o}$.

Then equations (23), (24) can be written as:

$$\frac{\partial}{\partial x}\left(\rho_o \lambda_{ox} \cdot \frac{\partial p_o}{\partial x}\right) + \frac{\partial}{\partial y}\left(\rho_o \lambda_{oy} \cdot \frac{\partial p_o}{\partial y}\right) = \frac{\partial\left(\rho_o \phi S_o\right)}{\partial t} \tag{37}$$

$$\frac{\partial}{\partial x}\left(\rho_w\lambda_{wx}\cdot\frac{\partial p_w}{\partial x}\right)+\frac{\partial}{\partial y}\left(\rho_o\lambda_{wy}\cdot\frac{\partial p_w}{\partial y}\right)=\frac{\partial\left(\rho_o\phi S_w\right)}{\partial t} \tag{38}$$

(The left end of Eq. (37) can be expanded as:

$$\nabla\left(\rho_o\frac{K\cdot K_r}{\mu_o}\nabla p_o\right)=\nabla\left(\rho_o\right)\cdot\frac{K\cdot K_r}{\mu_o}\nabla p_o+\rho_o\nabla\left(\frac{K\cdot K_r}{\mu_o}\nabla p_o\right) \tag{39}$$

When the fluid is effectively compressible, it can be ignored because of $\nabla\left(\rho_o\right)\cdot\frac{K\cdot K_r}{\mu_o}\nabla p_o\cdot\rho_o\nabla\left(\frac{K\cdot K_{ro}}{\mu_o}\nabla p_o\right)$.

Therefore there is:

$$\nabla\left(\rho_o\frac{K\cdot K_{ro}}{\mu_o}\nabla p_o\right)=\rho_o\nabla\left(\frac{K\cdot K_{ro}}{\mu_o}\nabla p_o\right) \tag{40}$$

The right end of Eq. (37) can be expanded as:

$$\begin{aligned}\frac{\partial\left(\phi S_o\rho_o\right)}{\partial t}&=S_o\rho_o\frac{\partial\phi}{\partial t}+S_o\phi\frac{\partial\rho_o}{\partial t}+\phi\rho_o\frac{\partial S_o}{\partial t}\\&=S_o\rho E\frac{\partial\phi}{\partial p_o}\frac{\partial p_o}{\partial t}+S_o\phi\frac{\partial\rho_o}{\partial p_o}\frac{\partial p_o}{\partial t}+\phi\rho_o\frac{\partial S_o}{\partial t}\end{aligned} \tag{41}$$

The relationship between porosity and pressure is given by the equation:

$$\phi=\phi_a\left[1+C_R\left(p-p_a\right)\right] \tag{42}$$

So:

$$\frac{\partial\phi}{\partial p}=\phi_a C_R \tag{43}$$

The compression factor is:

$$C_1=\frac{1}{\rho_1}\frac{\partial\rho_1}{\partial p_1}l=o,w \tag{44}$$

Since the fluid is slightly compressible, treat C_1 as a constant.
There:

$$\frac{\partial\rho_1}{\partial p_1}=C_1\rho_1 \tag{45}$$

From this it follows:

$$\frac{\partial\left(\phi S_o\rho_o\right)}{\partial t}=S_o\rho_o\phi_s C_R\frac{\partial p_o}{\partial t}+S_o\phi C_o\rho_o\frac{\partial p_o}{\partial t}+\phi\rho_o\frac{\partial S_o}{\partial t} \tag{46}$$

Then the oil phase equation (37) can be written as:

$$\nabla\left(\frac{K\cdot K_{ro}}{\mu_o}\nabla p_o\right)=S_o\phi_a C_R\frac{\partial p_o}{\partial t}+S_o\phi C_o\frac{\partial p_o}{\partial t}+\phi\frac{\partial S_o}{\partial t} \tag{47}$$

Similarly, the water phase equation (38) can be written as:

$$\nabla\left(\frac{K\cdot K_{rw}}{\mu_w}\nabla p_w\right)=S_w\phi_a C_R\frac{\partial p_w}{\partial t}+S_w\phi C_w\frac{\partial p_w}{\partial t}+\phi\frac{\partial S_w}{\partial t} \tag{48}$$

by the saturation relationship:

$$S_w + S_o = 1 \tag{49}$$

So:

$$\frac{\partial S_w}{\partial t} = -\frac{\partial S_o}{\partial t} \tag{50}$$

Adding (37) and (38) gives:

$$\begin{aligned}\nabla\left(\frac{K \cdot K_{rw}}{\mu_w}\nabla p_w\right) + \nabla\left(\frac{K \cdot K_{IO}}{\mu_o}\nabla p_o\right) = S_w \phi_a C_R \frac{\partial p_w}{\partial t} \\ + S_w \phi C_w \frac{\partial p_w}{\partial t} + S_o \phi_a C_R \frac{\partial p_o}{\partial t} + S_o \phi C_o \frac{\partial p_o}{\partial t}\end{aligned} \tag{51}$$

Then (47) can be written as:

$$\nabla\left(\frac{K \cdot K_{rw}}{\mu_w}\nabla p_w\right) + \nabla\left(\frac{K \cdot K_{ro}}{\mu_o}\nabla p_o\right) = \left(\phi_a C_R + S_w \phi C_w + S_o \phi C_o\right)\frac{\partial p_o}{\partial t} \tag{52}$$

Let $C_t = \frac{\phi_a}{\phi} C_R + S_w C_w + S_o C_o$, then the above equation is expressed as:

$$\begin{aligned}\nabla \cdot \left[\left(\frac{K \cdot K_{ro}}{\mu_o} + \frac{K \cdot K_{rw}}{\mu_w}\right)\nabla p_o - \frac{K \cdot K_{rw}}{\mu_w}\nabla p_c\left(S_w\right)\right] + \frac{q_o}{\rho_o} + \frac{q_w}{\rho_w} \\ = \phi C_t \frac{\partial p}{\partial t}\end{aligned} \tag{53}$$

Equation (53) is the oil phase pressure equation.

The right end of the water-phase equation (48) has the first term negligible due to $S_w\left(\phi_a C_R + \phi C_w\right)\frac{\partial p_w}{\partial t} \cdot \phi \frac{\partial S_w}{\partial t}$, so there is:

$$\nabla \cdot \left[\frac{K \cdot K_{rw}}{\mu_w}\nabla p_o - \frac{K \cdot K_{rw}}{\mu_w}\nabla p_c^{n+1}\left(S_w\right)\right] + \frac{q_w}{\rho_w} = \phi \frac{\partial S_w}{\partial t} \tag{54}$$

Where: $p_c^{n+1}\left(S_w\right)$, $\frac{p_c}{S_w} S_w^{n+1}$, $p_c^n \cdot \frac{p_c}{S_w} S_w^n$, Eq. n is the previous iteration step and $n+1$ is the current iteration step, Eq. (54) is the water phase saturation equation.

2.2.2. Finite element equations for oil phase pressure.Let the shape function vector be:

$$N = \left(N_1, N_2 \ldots N_n\right) \tag{55}$$

The trial solution for the oil phase pressure is:

$$\tilde{p} = \sum_{i=1}^{n} N_t p_t \tag{56}$$

The coordinates within the cell:

$$x = \sum_{i=1}^{n} N_t x_i \tag{57}$$

$$y = \sum_{i=1}^{n} N_i y_i \tag{58}$$

Where: n is the number of nodes in the cell, p_i is the pressure value at the cell node, x_i, y_i are the horizontal and vertical coordinates of the cell node.

Integrating the oil phase pressure equation (54) within each cell yields:

$$\begin{aligned}&\iint_e N_i\left[\nabla\left(\frac{K\cdot K_{rw}}{\mu_w}\nabla p\right)+\nabla\left(\frac{K\cdot K_{ro}}{\mu_o}\nabla p\right)-\frac{K\cdot K_{rw}}{\mu_w}\nabla P_c\left(S_w\right)\right]\\&dxdy=\iint_e N_i\phi C_t\frac{\partial p}{\partial t}dxdy\end{aligned}\tag{59}$$

The above equation can be expressed as:

$$\begin{aligned}&\iint_e N_i\left[\frac{\partial}{\partial x}\left(\lambda_{ox}\frac{\partial\tilde{p}}{\partial x}\right)+\frac{\partial}{\partial y}\left(\lambda_{oy}\frac{\partial\tilde{p}}{\partial y}\right)+\frac{\partial}{\partial x}\left(\lambda_{wx}\frac{\partial\tilde{p}}{\partial x}\right)\right.\\&\left.+\frac{\partial}{\partial y}\left(\lambda_{wy}\frac{\partial\tilde{p}}{\partial y}\right)-\frac{\partial}{\partial x}\left(\lambda_{wx}\frac{\partial p_c}{\partial x}\right)+\frac{\partial}{\partial y}\left(\lambda_{wy}\frac{\partial p_c}{\partial y}\right)\right]dxdy\\&=\iint_e N_i\phi C_t\frac{\partial\tilde{p}}{\partial t}dxdy\end{aligned}\tag{60}$$

Partial integration of the above equation in order to obtain the weak solution form, the first two terms at the left end can be expressed as:

$$\begin{aligned}&\iint N_i\left[\frac{\partial}{\partial x}\left(\lambda_{ox}\frac{\partial\tilde{p}}{\partial x}\right)+\frac{\partial}{\partial y}\left(\lambda_{oy}\frac{\partial\tilde{p}}{\partial y}\right)\right]dxdy\\&=-\iint\left[\frac{\partial N_i}{\partial x}\cdot\lambda_{ox}\frac{\partial\tilde{p}}{\partial x}-\frac{\partial N_i}{\partial y}\cdot\lambda_{oy}\frac{\partial\tilde{p}}{\partial y}\right]dxdy\\&+\prod_{\Gamma}N_i\left(\lambda_{ox}n_x\partial+\lambda_{oy}n_y\frac{\partial\tilde{p}}{\partial y}\right)d\Gamma\end{aligned}\tag{61}$$

Where: n_x, n_y is the directional cosine of the normal outside the boundary.

Let:

$$v_o=\frac{K\cdot K_{ro}}{\mu_o r\ln\frac{r}{r_w}}p_{wf};v_w=\frac{K\cdot K_{rv}}{\mu_w r\ln\frac{r}{r_w}}p_{wf}\tag{62}$$

The second term at the right end is the loop integral along the cell boundary. This integral is equal to zero for the inner cell and for the outer boundary cell with closed conditions. Substitute Eqs. N, $\tilde{p}$, x, and y into (62) and write it in matrix form:

$$\iint N_i\left[\frac{\partial}{\partial x}\left(\lambda_{ox}\frac{\partial\tilde{p}}{\partial x}\right)+\frac{\partial}{\partial y}\left(\lambda_{oy}\frac{\partial\tilde{p}}{\partial y}\right)\right]dxdy$$

$$= -\iint\begin{pmatrix}\frac{\partial N_1}{\partial x} & \frac{\partial N_1}{\partial y}\\ \frac{\partial N_2}{\partial x} & \frac{\partial N_2}{\partial y}\\ \vdots & \vdots\\ \frac{\partial N_n}{\partial x} & \frac{\partial N_n}{\partial y}\end{pmatrix}\begin{pmatrix}\lambda_{ox} & 0\\ 0 & \lambda_{oy}\end{pmatrix}\begin{pmatrix}\frac{\partial N_1}{\partial x} & \frac{\partial N_2}{\partial x} & \cdots & \frac{\partial N_n}{\partial x}\\ \frac{\partial N_1}{\partial y} & \frac{\partial N_1}{\partial y} & \cdots & \frac{\partial N_n}{\partial y}\end{pmatrix}$$

$$\begin{pmatrix}p_1\\ p_2\\ \vdots\\ p_n\end{pmatrix}dxdy+\int_{\Gamma 2}N^T q_{oi}d\Gamma \tag{63}$$

$$-\int_{\Gamma 1}\begin{pmatrix}N_1\\ N_2\\ \vdots\\ N_n\end{pmatrix}\begin{pmatrix}\lambda_{ox}\cdot\frac{1}{r\cdot\ln\frac{r}{r_w}} & 0\\ 0 & \lambda_{oy}\cdot\frac{1}{r\cdot\ln\frac{r}{r_w}}\end{pmatrix}\begin{pmatrix}\frac{\partial N_1}{\partial x} & \frac{\partial N_2}{\partial x} & \cdots & \frac{\partial N_n}{\partial x}\\ \frac{\partial N_1}{\partial y} & \frac{\partial N_1}{\partial y} & \cdots & \frac{\partial N_n}{\partial y}\end{pmatrix}$$

$$\begin{pmatrix}p_1\\ p_2\\ \vdots\\ p_n\end{pmatrix}d\Gamma+\left[\int_{\Gamma 1}\begin{pmatrix}N_1\\ N_2\\ \vdots\\ N_n\end{pmatrix}v_o d\Gamma\right.$$

$$= -\left(\iint B^T T_0 B\,dx\,dy\right)\cdot P-\left(\int_{\Gamma 1}N^T T_{o\tau}B\,d\Gamma\right)\cdot P$$

$$+\int_{\Gamma 1}N^T v_0\,d\Gamma+\int_{\Gamma 2}N^T q_{oi}\,d\Gamma$$

Among them:

$B=\begin{pmatrix}\frac{\partial N_1}{\partial x} & \frac{\partial N_2}{\partial x} & \cdots & \frac{\partial N_n}{\partial x}\\ \frac{\partial N_1}{\partial y} & \frac{\partial N_2}{\partial y} & \cdots & \frac{\partial N_n}{\partial y}\end{pmatrix}=J^{-1}\begin{pmatrix}\frac{\partial N_1}{\partial \xi} & \frac{\partial N_2}{\partial \xi} & \cdots & \frac{\partial N_n}{\partial \xi}\\ \frac{\partial N_1}{\partial \eta} & \frac{\partial N_2}{\partial \eta} & \cdots & \frac{\partial N_n}{\partial \eta}\end{pmatrix}$, q_{oi} are the oil phase flow rates at the bottom of the well:

$J\equiv\frac{\partial(x,y)}{\partial(\xi,\eta)}=\begin{pmatrix}\frac{\partial N_1}{\partial \xi} & \frac{\partial N_2}{\partial \xi} & \cdots & \frac{\partial N_n}{\partial \xi}\\ \frac{\partial N_1}{\partial \eta} & \frac{\partial N_2}{\partial \eta} & \cdots & \frac{\partial N_n}{\partial \eta}\end{pmatrix}\begin{pmatrix}x_1 & y_1\\ x_2 & y_2\\ \vdots & \vdots\\ x_n & y_n\end{pmatrix}$, is the Jacobi matrix;

$$T_o = \begin{pmatrix} \lambda_{ox} & 0 \\ 0 & \lambda_{ox} \end{pmatrix};\ T_{o\tau} = \begin{pmatrix} \lambda_{ox} \cdot \dfrac{1}{r \cdot \ln \dfrac{r}{r_w}} & 0 \\ 0 & \lambda_{ox} \cdot \dfrac{1}{r \cdot \ln \dfrac{r}{r_w}} \end{pmatrix} P = \begin{pmatrix} p_1 \\ p_2 \\ \vdots \\ p_n \end{pmatrix}$$ is the junction pressure vector.

$$dxdy = |J|\, d\xi\, d\zeta \tag{64}$$

Using the same process as above, the third and fourth terms at the left end of Eq. (60) become:

$$\begin{aligned}
&\iint N_i \left[\frac{\partial}{\partial x}\left(\lambda_{wx} \frac{\partial \tilde{p}}{\partial x} \right) + \frac{\partial}{\partial y}\left(\lambda_{wy} \frac{\partial \tilde{p}}{\partial y} \right) \right] dxdy \\
&= -\iint \begin{pmatrix} \frac{\partial N_1}{\partial x} & \frac{\partial N_1}{\partial y} \\ \frac{\partial N_2}{\partial x} & \frac{\partial N_2}{\partial y} \\ \vdots & \vdots \\ \frac{\partial N_n}{\partial x} & \frac{\partial N_n}{\partial y} \end{pmatrix} \begin{pmatrix} \lambda_{wx} & 0 \\ 0 & \lambda_{wy} \end{pmatrix} \begin{pmatrix} \frac{\partial N_1}{\partial x} & \frac{\partial N_2}{\partial x} & \cdots & \frac{\partial N_n}{\partial x} \\ \frac{\partial N_1}{\partial y} & \frac{\partial N_2}{\partial y} & \cdots & \frac{\partial N_n}{\partial y} \end{pmatrix} \\
&\begin{pmatrix} p_1 \\ p_2 \\ \vdots \\ p_n \end{pmatrix} dxdy + \int_{\Gamma 2} N^{\tau} q_{wi} d\Gamma - \int_{\Gamma 1} \begin{pmatrix} N_1 \\ N_2 \\ \vdots \\ N_n \end{pmatrix} \\
&\begin{pmatrix} \lambda_{wx} \cdot \dfrac{1}{r \cdot \ln \dfrac{r}{r_w}} & 0 \\ 0 & \lambda_{wy} \cdot \dfrac{1}{r \cdot \ln \dfrac{r}{r_w}} \end{pmatrix} \begin{pmatrix} \frac{\partial N_1}{\partial x} & \frac{\partial N_2}{\partial x} & \cdots & \frac{\partial N_n}{\partial x} \\ \frac{\partial N_1}{\partial y} & \frac{\partial N_1}{\partial y} & \cdots & \frac{\partial N_n}{\partial y} \end{pmatrix} \\
&\begin{pmatrix} p_1 \\ p_2 \\ \vdots \\ p_n \end{pmatrix} d\Gamma + \int_{\Gamma 1} \begin{pmatrix} N_1 \\ N_2 \\ \vdots \\ N_n \end{pmatrix} v_w d\Gamma \\
&= -\left(\iint B^T T_w B\, dx\, dy \right) \cdot P - \left(\int_{\Gamma 1} N^T T_{wz} B\, d\Gamma \right) \cdot P \\
&+ \int_{\Gamma 1} N^T v_w\, d\Gamma + \int_{\Gamma 2} N^T q_{wi}\, d\Gamma
\end{aligned} \tag{65}$$

Of which: $T_w = \begin{pmatrix} \lambda_{wx} & 0 \\ 0 & \lambda_{wy} \end{pmatrix};\ T_{w\tau} = \begin{pmatrix} \lambda_{wx} \cdot \dfrac{1}{r \cdot \ln \dfrac{r}{r_w}} & 0 \\ 0 & \lambda_{wx} \cdot \dfrac{1}{r \cdot \ln \dfrac{r}{r_w}} \end{pmatrix}$

The fourth and fifth items are:

$$\iint N_i\left[\frac{\partial}{\partial x}\left(\lambda_{wx}\frac{\partial p_c}{\partial x}\right)+\frac{\partial}{\partial y}\left(\lambda_{wy}\frac{\partial p_c}{\partial y}\right)\right]dxdy$$
$$=-\iint\begin{pmatrix}\frac{\partial N_1}{\partial x} & \frac{\partial N_t}{\partial y}\\ \frac{\partial N_2}{\partial x} & \frac{\partial N_2}{\partial y}\\ \vdots & \vdots\\ \frac{\partial N_n}{\partial x} & \frac{\partial N_n}{\partial y}\end{pmatrix}\begin{pmatrix}\lambda_{wx} & 0\\ 0 & \lambda_{wy}\end{pmatrix}\begin{pmatrix}\frac{\partial N_1}{\partial x} & \frac{\partial N_2}{\partial x} & \cdots & \frac{\partial N_n}{\partial x}\\ \frac{\partial N_1}{\partial y} & \frac{\partial N_2}{\partial y} & \cdots & \frac{\partial N_n}{\partial y}\end{pmatrix} \tag{66}$$
$$\begin{pmatrix}p_{c1}\\ p_{c2}\\ \vdots\\ p_{cn}\end{pmatrix}dxdy=-\left(\iint B^T T_w B dxdy\right)\cdot P_c\left(S_w\right)$$

Then the right end of equation (60) becomes:

$$\iint_e N_i\phi C_t\frac{\partial\tilde{p}}{\partial t}dxdy=\iint_e\begin{pmatrix}N_1\\ N_2\\ \vdots\\ N_n\end{pmatrix}\phi C_t\begin{pmatrix}N_1\\ N_2\\ \vdots\\ N_n\end{pmatrix}^T\begin{pmatrix}\frac{\partial p_1}{\partial t}\\ \frac{\partial p_2}{\partial t}\\ \vdots\\ \frac{\partial p_n}{\partial t}\end{pmatrix}dxdy \tag{67}$$
$$=\left(\iint_e\phi C_t N^T N dxdy\right)\frac{\partial P}{\partial t}$$

Then equation (60) becomes:

$$\begin{aligned}&\left(\iint_e B^T\left(T_o+T_w\right)Bdxdy+\iint_{\Gamma 1}N^T\left(T_{or}+T_{w\tau}\right)Bd\Gamma\right)\cdot P\\ &+\left(\iint_e\phi C_i N^T N dxdy\right)\frac{\partial P}{\partial t}\\ &=\int_{\Gamma 2}N^T\left(q_{oi}+q_{wi}\right)d\Gamma+\int_{\Gamma 1}N^T\left(v_0+v_w\right)d\Gamma\\ &+\iint_e B^T T_n B dxdy\cdot P_c\left(S_w\right)\end{aligned} \tag{68}$$

If we set $K_{ep}=\iint_e B^T\left(T_o+T_w\right)Bdxdy+\int_\Gamma N^T\left(T_{or}+T_{w\tau}\right)Bd\Gamma$, $C_{ep}=\iint_e\phi C_t N^T N dxdy$, $F_{ep}=\iint_{\Gamma 1}N^T\left(v_o+v_w\right)d\Gamma+\iint_{\Gamma 2}N^T\left(q_{oi}+q_{wi}\right)d\Gamma+\iint_e B^T T_w B dxdy\cdot P_c\left(S_w\right)$

Then (68) can be written as:

$$K_{ep}P+C_{ep}\frac{\partial P}{\partial t}=F_{ep} \tag{69}$$

Eq. (69) is the finite element unit balance equation for oil phase pressure.

2.2.3. Finite element equation for aqueous phase saturation. In addition to defining the shape function, the trial solution for the oil phase pressure, and the coordinates within the cell, the trial solution for the water phase saturation is also defined as:

$$\tilde{S} = \sum_{i=1}^{n} N_i S_i \tag{70}$$

Substituting the shape function, the trial solution for the oil phase pressure, the trial solution for the water phase saturation, and the coordinates in the cell into the saturation equation gives:

$$\begin{aligned}
&\frac{\partial}{\partial x}\left(\lambda_{wx}\frac{\partial \tilde{p}}{\partial x}\right)+\frac{\partial}{\partial y}\left(\lambda_{wy}\frac{\partial \tilde{p}}{\partial y}\right)-\frac{\partial}{\partial x}\left(\lambda_{wx}\cdot\frac{\partial p_c}{\partial s_w}\cdot\frac{\partial \tilde{S}}{\partial x}\right)\\
&-\frac{\partial}{\partial y}\left(\lambda_{wy}\frac{\partial p_c}{\partial S_w}\cdot\frac{\partial \tilde{S}}{\partial y}\right)-\frac{\partial}{\partial x}\left(\lambda_{wx}\frac{\partial p_c^n}{\partial x}\right)-\frac{\partial}{\partial y}\left(\lambda_{wy}\frac{\partial p_c^n}{\partial y}\right)\Bigg]\\
&+\frac{\partial}{\partial x}\left(\lambda_{wx}\cdot\frac{\partial p_c}{\partial S_w}\cdot\frac{\partial \tilde{S}^n}{\partial x}\right)+\frac{\partial}{\partial y}\left(\lambda_{wy}\frac{\partial p_c}{\partial S_w}\cdot\frac{\partial \tilde{S}^n}{\partial y}\right)\\
&=\phi\frac{\partial \tilde{S}}{\partial t}
\end{aligned} \tag{71}$$

where: superscript n represents the previous iteration step. The cell analysis is performed first. The equivalent integral form of (71) is obtained by integrating within the cell by Galerkin's method [29] as:

$$\begin{aligned}
&\iint_e N_i\left[\frac{\partial}{\partial x}\left(\lambda_{wx}\frac{\partial \tilde{p}}{\partial x}\right)+\frac{\partial}{\partial y}\left(\lambda_{wy}\frac{\partial \tilde{p}}{\partial y}\right)-\frac{\partial}{\partial x}\left(\lambda_{wx}\cdot\frac{\partial p_c}{\partial s_w}\cdot\frac{\partial \tilde{S}}{\partial x}\right)\right.\\
&-\frac{\partial}{\partial y}\left(\lambda_{wy}\frac{\partial p_c}{\partial S_w}\cdot\frac{\partial \tilde{S}}{\partial y}\right)-\frac{\partial}{\partial x}\left(\lambda_{wx}\frac{\partial p_c{}^n}{\partial x}\right)-\frac{\partial}{\partial y}\left(\lambda_{wy}\frac{\partial p_c{}^n}{\partial y}\right)\\
&\left.+\frac{\partial}{\partial x}\left(\lambda_{wx}\cdot\frac{\partial p_c}{\partial S_w}\cdot\frac{\partial \tilde{S}^n}{\partial x}\right)+\frac{\partial}{\partial y}\left(\lambda_{wy}\frac{\partial p_c}{\partial S_w}\cdot\frac{\partial \tilde{S}^n}{\partial y}\right)\right]dxdy\\
&=\iint_c N_i\phi\frac{\partial \tilde{S}'}{\partial t}dxdy
\end{aligned} \tag{72}$$

Division Points Score:

$$
\begin{aligned}
&-\iint \begin{pmatrix} \frac{\partial N_1}{\partial x} & \frac{\partial N_1}{\partial y} \\ \frac{\partial N_2}{\partial x} & \frac{\partial N_2}{\partial y} \\ \vdots & \vdots \\ \frac{\partial N_n}{\partial x} & \frac{\partial N_n}{\partial y} \end{pmatrix} \begin{pmatrix} \lambda_{wx} & 0 \\ 0 & \lambda_{wy} \end{pmatrix} \begin{pmatrix} \frac{\partial N_1}{\partial x} & \frac{\partial N_2}{\partial x} & \cdots & \frac{\partial N_n}{\partial x} \\ \frac{\partial N_1}{\partial y} & \frac{\partial N_2}{\partial y} & \cdots & \frac{\partial N_n}{\partial y} \end{pmatrix} \begin{pmatrix} p_1 \\ p_2 \\ \vdots \\ p_n \end{pmatrix} dxdy + \int_{\Gamma 2} N^T q_{wi} d\Gamma - \\
&\int_{\Gamma 1} \begin{pmatrix} N_1 \\ \Pi \\ N_2 \\ \vdots \\ N_n \end{pmatrix} \begin{pmatrix} \lambda_{wx} \cdot \frac{1}{r \cdot \ln \frac{r}{r_w}} & 0 \\ 0 & \lambda_{wy} \cdot \frac{1}{r \cdot \ln \frac{r}{r_w}} \end{pmatrix} \begin{pmatrix} \frac{\partial N_1}{\partial x} & \frac{\partial N_2}{\partial x} & \cdots & \frac{\partial N_a}{\partial x} \\ \frac{\partial N_1}{\partial y} & \frac{\partial N_1}{\partial y} & \cdots & \frac{\partial N_a}{\partial y} \end{pmatrix} \begin{pmatrix} p_1 \\ p_2 \\ \vdots \\ p_n \end{pmatrix} d\Gamma\Gamma + \int_{\Gamma 1} \begin{pmatrix} N_1 \\ N_2 \\ \vdots \\ N_n \end{pmatrix} v_w d\Gamma + \\
&\iint \begin{pmatrix} \frac{\partial N_1}{\partial x} & \frac{\partial N_1}{\partial y} \\ \frac{\partial N_2}{\partial x} & \frac{\partial N_2}{\partial y} \\ \vdots & \vdots \\ \frac{\partial N_0}{\partial x} & \frac{\partial N_n}{\partial y} \end{pmatrix} \begin{pmatrix} \lambda_{wx} \cdot \frac{\partial p_c}{\partial S_w} & 0 \\ 0 & \lambda_{wy} \cdot \frac{\partial p_c}{\partial S_w} \end{pmatrix} \begin{pmatrix} \frac{\partial N_1}{\partial x} & \frac{\partial N_2}{\partial x} & \cdots & \frac{\partial N_n}{\partial x} \\ \frac{\partial N_1}{\partial y} & \frac{\partial N_2}{\partial y} & \cdots & \frac{\partial N_n}{\partial y} \end{pmatrix} \begin{pmatrix} S_1 \\ S_2 \\ \vdots \\ S_n \end{pmatrix} dxdy + \\
&\iint \begin{pmatrix} \frac{\partial N_1}{\partial x} & \frac{\partial N_1}{\partial y} \\ \frac{\partial N_2}{\partial x} & \frac{\partial N_2}{\partial y} \\ \vdots & \vdots \\ \frac{\partial N_n}{\partial x} & \frac{\partial N_n}{\partial y} \end{pmatrix} \begin{pmatrix} \lambda_{wx} & 0 \\ 0 & \lambda_{wy} \end{pmatrix} \begin{pmatrix} \frac{\partial N_1}{\partial x} & \frac{\partial N_2}{\partial x} & \cdots & \frac{\partial N_n}{\partial x} \\ \frac{\partial N_1}{\partial y} & \frac{\partial N_2}{\partial y} & \cdots & \frac{\partial N_n}{\partial y} \end{pmatrix} \begin{pmatrix} p_{cc} \\ p_{cz} \\ \vdots \\ p_{cn} \end{pmatrix} dxdy - \\
&\iint \begin{pmatrix} \frac{\partial N_1}{\partial x} & \frac{\partial N_1}{\partial y} \\ \frac{\partial N_2}{\partial x} & \frac{\partial N_2}{\partial y} \\ \vdots & \vdots \\ \frac{\partial N_a}{\partial x} & \frac{\partial N_a}{\partial y} \end{pmatrix} \begin{pmatrix} \lambda_{wx} \cdot \frac{\partial p_c}{\partial s_w} & 0 \\ 0 & \lambda_{wy} \cdot \frac{\partial p_c}{\partial s_w} \end{pmatrix} \begin{pmatrix} \frac{\partial N_1}{\partial x} & \frac{\partial N_2}{\partial x} & \cdots & \frac{\partial N_a}{\partial x} \\ \frac{\partial N_1}{\partial y} & \frac{\partial N_2}{\partial y} & \cdots & \frac{\partial N_n}{\partial y} \end{pmatrix} \begin{pmatrix} S_1^n \\ S_2^n \\ \vdots \\ S_n^n \end{pmatrix} dxdy \\
&= \iint_e \begin{pmatrix} N_1 \\ N_2 \\ \vdots \\ N_n \end{pmatrix} \phi \begin{pmatrix} N_1 \\ N_2 \\ \vdots \\ N_n \end{pmatrix}^T \begin{pmatrix} \frac{\partial S_1}{\partial t} \\ \frac{\partial S_2}{\partial t} \\ \vdots \\ \frac{\partial S_n}{\partial t} \end{pmatrix} dxdy
\end{aligned}
\tag{73}
$$

Organized:

$$\begin{aligned}&\left(\iint_e NN\phi dxdy\right)\cdot\frac{\partial S}{\partial t}-\iint_e B^T TBdxdy\cdot S\\&=-\left(\iint_e B^T T_w Bdxdy+\int_{\Gamma 1}N^T T_{w\tau}Bd\Gamma\right)\cdot P\\&+\int_{\Gamma 1}Nv_w d\Gamma+\iint B^T T_w Bdxdy\cdot P_c\left(S_w\right)\\&-\iint_e B^T TBdxdy\cdot S^n+\iint_{\Gamma 2}Nq_{wi}d\Gamma\end{aligned}\tag{74}$$

Of which: $T=\begin{pmatrix}\lambda_{wx}\cdot\dfrac{\partial p_e}{\partial s_w} & 0\\ 0 & \lambda_{wy}\cdot\dfrac{\partial p_e}{\partial s_w}\end{pmatrix}$, Order:

$$\begin{aligned}F_{es}&=-\left(\iint_e B^T T_w Bdxdy+\int_{\Gamma 1}N^T T_w Bd\Gamma\right)\cdot P\\&+\int_{\Gamma 1}N^T v_w d\Gamma+\iint B^T T_w Bdxdy\cdot P_c\left(S_w\right)\\&-\iint_e B^T TBdxdy\cdot S^n+\int_{\Gamma 2}N^T q_w d\Gamma\\C_e&=\iint_e N^T N\phi dxdy,K_e=-\iint_e B^T TBdxdy\end{aligned}\tag{75}$$

Substituting into (74) yields:

$$C_{es}\frac{\partial S}{\partial t}+K_{es}S=F_{es}\tag{76}$$

which is the finite element unit balance equation for the saturation of the aqueous phase.

3. Analysis of the results of numerical simulation and optimization of pressure in the oil seepage field

3.1. *Research on the coupling law of seepage field and stress field*

3.1.1. Reservoir Rock Stress-Strain Change Laws. Figure 2 shows the stress distribution map at 300 days of development, where (a) and (b) represent the minimum and maximum principal stress distribution maps, respectively, in MPa. Figure 3 shows the curve of rock strain with space in the wellbore network; Figure 4 shows the curve of rock strain with time in the wellbore network. The changing rule of reservoir stress-strain with space is: the amount of change near the borehole is larger, and the gradient of change is also obviously larger. The amount of change toward the reservoir boundary decreases quickly. The stress-strain has a larger area of influence within the control range of the well. In terms of time, the amount of change in stress-strain at each point of the reservoir decreases and stabilizes with production time. From the analysis, it can be seen that the change of stress-strain is due to the change of fluid pressure. The larger the fluid pressure gradient is, the larger the amount of stress-strain change is. In the original state, the fluid pressure and ground stress are equal at each point of the reservoir, and the rock strain can be considered to be zero. When the oil well is set to bottomhole differential pressure production, a large fluid pressure gradient is formed near the bottom of the well, and the fluid pressure gradient toward the reservoir boundary decreases quickly. Therefore, the fluid-solid coupling effect is stronger at the bottom of the well and decreases more quickly toward the reservoir boundary. The amount of stress-strain change caused by fluid-solid coupling is larger at the bottom of the well and decreases quickly toward the reservoir boundary. Temporally, the pressure gradient near the bottom of the well is very large at the beginning of production, and the amount of stress-strain change is large; subsequently, under the coupling effect, the fluid pressure gradient changes less, and the amount of stress-strain change decreases accordingly. It is conceivable that by the infinity production time, the fluid-solid coupling effect reaches equilibrium everywhere in the reservoir, so the fluid pressure and stress-strain no longer change. As the stress-strain of reservoir rock near the bottom of the well is large, it may damage the pore structure in this area, reduce the effective permeability, or even cause the rock to break out of the sand, reservoir collapse and other phenomena. To prevent such problems from occurring, large pressure gradients should be avoided in the area near the bottom of the well. This requires that the production regime should not be changed suddenly and drastically.

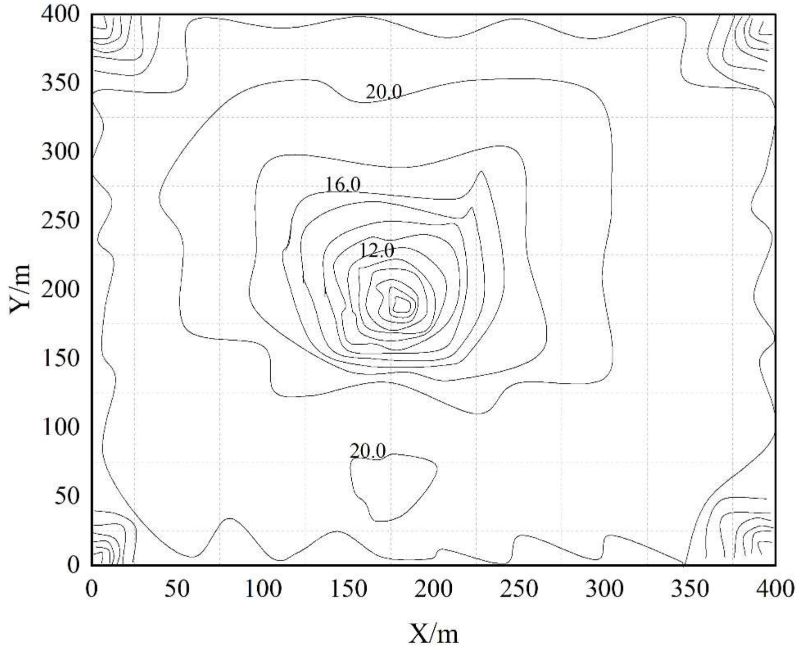

(a)Minimum principal stress profile

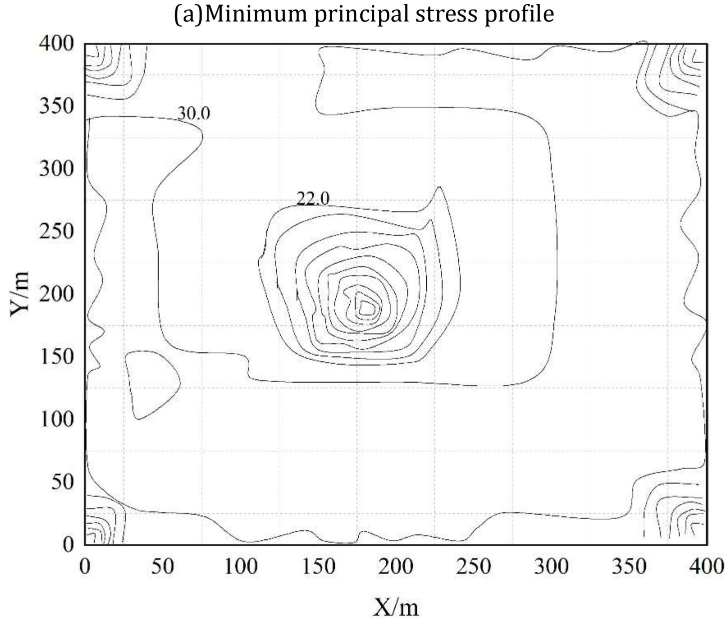

(b)Maximum principal stress profile

Fig. 2. Develop the minimum and maximum stress profile of 300 days (unit:MPa)

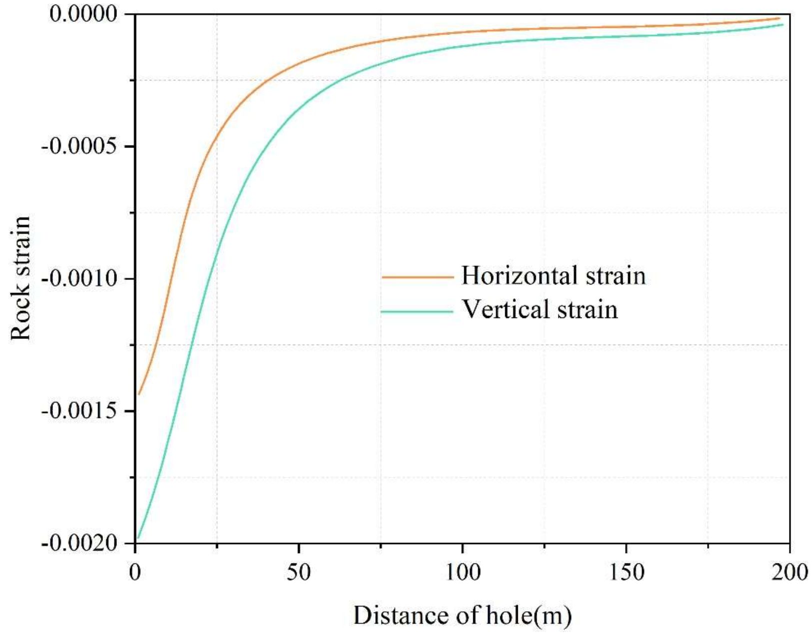

Fig. 3. The curve of the rock strain of the well of the shaft

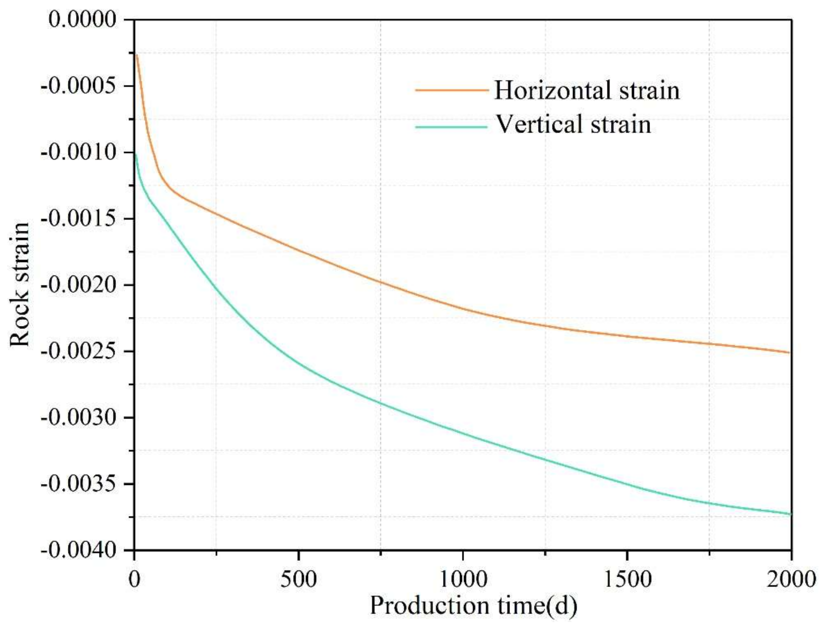

Fig. 4. The curve of the change of the rock strain at any time

3.1.2. Changing pattern of porosity and permeability. The curves of wellbore grid porosity and permeability with spatial loss are shown in Figure 5; the curves of wellbore grid porosity and permeability with time loss are shown in Figure 6. The change in porosity and permeability due to strain in the rock results in a change in the pore structure, which results in a change in the effective permeability. Therefore, the change rule of reservoir stress-strain with time and space determines the change characteristics of porosity and permeability with time and space.

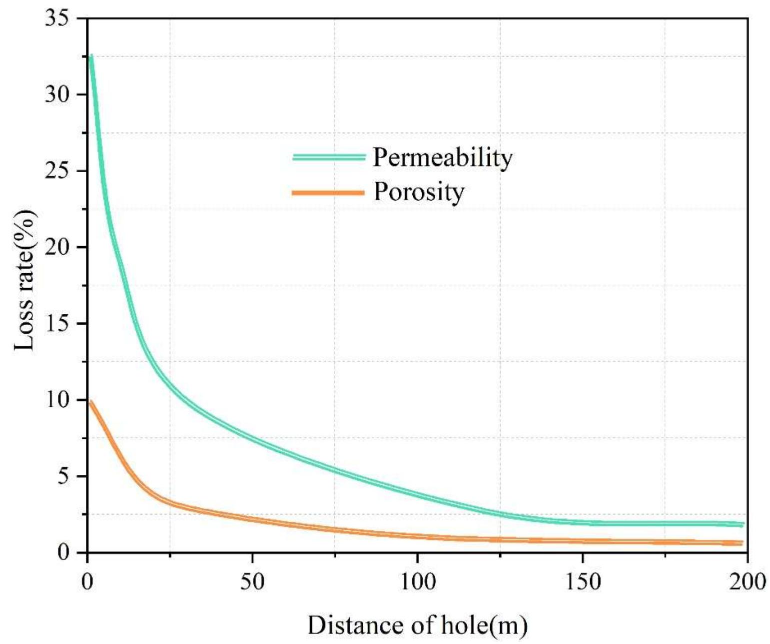

Fig. 5. The porosity of the well and the loss curve of permeability with the space

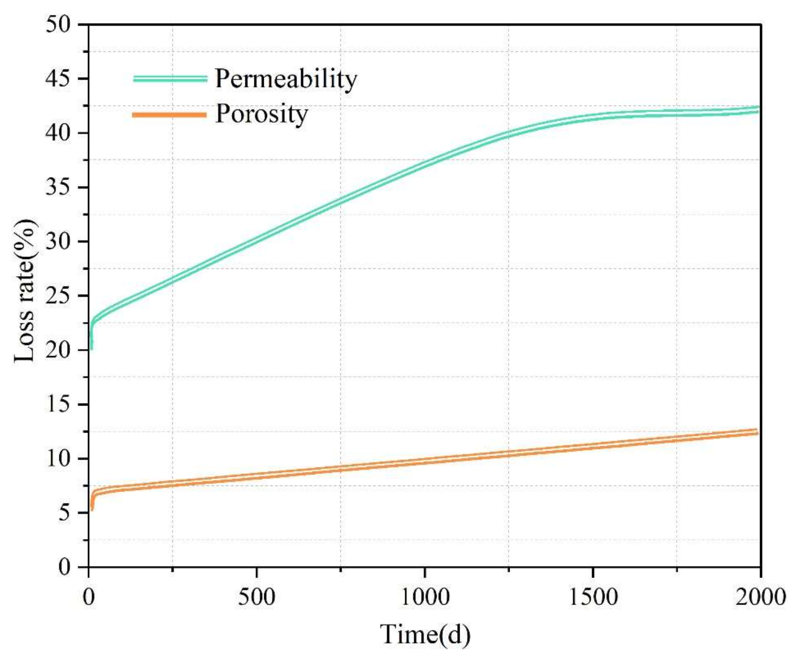

Fig. 6. The loss of the porosity and permeability of the wellbore grid

3.1.3. Changing patterns of development indicators. The results of the variation of the degree of extraction with time are shown in Fig. 7. The effect of reservoir rock deformation on production is shown in the following: on the one hand, the contraction of the rock will increase the elastic energy of the reservoir and increase the production; on the other hand, the deformation and contraction of the rock will inevitably decrease the permeability and porosity of the reservoir. Therefore, the production will decrease after considering the permeability and porosity affected by stress and strain. Theoretical analysis, experimental results and field practice show that sometimes porosity and permeability are greatly affected by stress-strain, which has a large impact on the development index calculated by simulation, and the calculated yield of the coupled model may be much lower than the predicted yield value of the uncoupled model. Therefore, in the numerical simulation of low-permeability reservoirs, the flow-solid coupling effect cannot be ignored.

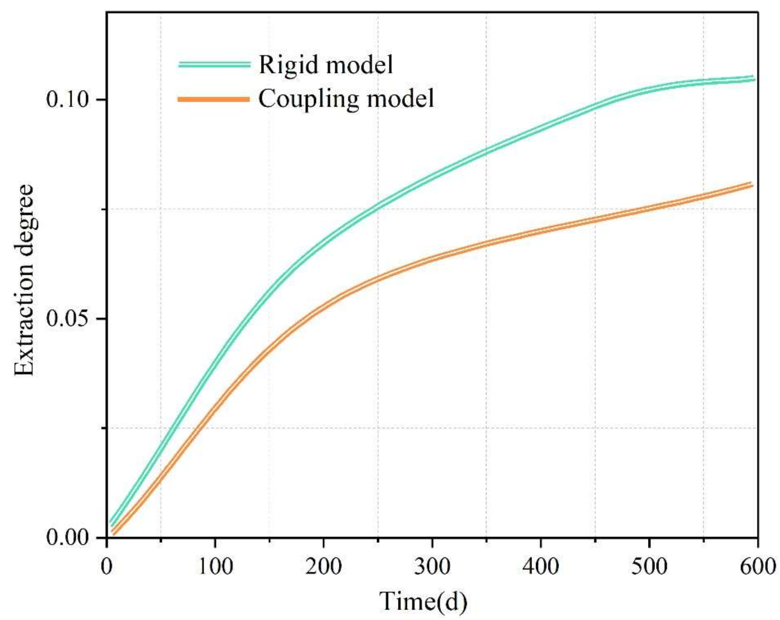

Fig. 7. The degree of recovery changes at any time

3.2. Mathematical modeling and solution of fractured horizontal wells

3.2.1. Mathematical modeling of stratigraphic percolation. Based on the understanding of the process of reserve utilization for elastic development of fractured horizontal wells, the Warren-Root model is used to establish an unstable seepage model for fractured horizontal wells in extra-low-permeability reservoirs under the consideration of start-up pressure gradient [30], and the basic seepage mechanics theories such as the principle of superposition of pressure drop and the line-source function are utilized, and the Laplace transform, Stehfest numerical inversion and other methods are applied to calculate and determine the fractured horizontal wells' Pressure distribution.

Define the uncaused variables as follows:

Uncausal pressure:

$$p_{ID} = \frac{2\pi k_{fh} h\left(p_i - p_i\right)}{q_{sc}\mu} \tag{77}$$

No causal distance:

$$r_D = \frac{r}{L_r} \tag{78}$$

No cause time:

$$t_D = \frac{k_{fi} t}{\mu\left(c_f \phi_f + c_m \phi_m\right) L_r^2} \tag{79}$$

Causeless start-up pressure:

$$G_D = \frac{2\pi k_{fi} h L_r G}{q_{sc}\mu} \tag{80}$$

No causal fracture conductivity:

$$C_{FD} = \frac{k_F w_F}{k_f h} \tag{81}$$

Elastic storage capacity ratio:

$$\omega = \frac{C_f \phi_f}{C_f \phi_f + C_m \phi_{mt}} \tag{82}$$

Fugitive coefficients:

$$\lambda = \frac{\sigma k_m L_r^{\ 2}}{k_f} \tag{83}$$

p_i -- Original stratigraphic pressure, MPa;
p_l -- formation pressure, MPa;
G --initiation pressure gradient, MPa/m;
h --Reservoir thickness, m;
L_r --reference length, m;
q_{sc} --yield, m^3/s;
k_F --hydraulic fracture permeability, μm^2;
k_{fi} --natural fracture original permeability, μm^2;
w_F --Width of hydraulic fracture, m;
C_f --Rock compression coefficient of the natural fracture system, MPa^{-1};
C_{mt} --Matrix system rock compression coefficient, MPa^{-1};
ϕ_f --Porosity of the natural fracture system, decimals;
ϕ_{mt} --Matrix system porosity, decimal;
σ --Shape factor, m^{-2}.

The continuity equation, the equation of motion, the equation of state, and the scuttling equation are combined to obtain the differential equation of seepage for a natural fracture system in a low-permeability dual-media reservoir:

$$\frac{1}{r}\frac{\partial}{\partial r}\left[r\frac{k_i}{\mu_o}\left(\frac{\partial p_f}{\partial r} - G\right)\right] + \frac{\alpha k_m}{\mu_o}\left(p_m - p_f\right) = 0 \tag{84}$$

Collating equation (89) yields:

$$\frac{1}{r}\left(\frac{k_i}{\mu_o}\frac{\partial p_f}{\partial r} + \frac{k_i}{\mu_o}\cdot r\frac{\partial^2 p_f}{\partial r^2} - \frac{k_i}{\mu_o}G\right) + \frac{\alpha k_m}{\mu_o}\left(p_m - p_f\right) = 0 \tag{85}$$

The simplification yields:

$$\frac{\partial^2 p_f}{\partial r^2} + \frac{1}{r}\frac{\partial p_f}{\partial r} - \frac{1}{r}G + \frac{\alpha k_m}{k_f}\left(p_m - p_f\right) = 0 \tag{86}$$

The differential equation for seepage in natural fracture systems is factorless as:

$$\frac{\partial^2 p_{fD}}{\partial r_D^2} + \frac{1}{r_D}\frac{\partial p_{fD}}{\partial r_D} + \frac{G_D}{r_D} - \lambda k_m\left(p_{mD} - p_{fD}\right) - \omega\frac{\partial p_{fD}}{\partial t_D} = 0 \tag{87}$$

Similarly, the differential equation for the seepage of the matrix system is:

$$\phi_m C_m \frac{\partial p_m}{\partial t} + \frac{\alpha k_m}{\mu_o}\left(p_m - p_f\right) = 0 \tag{88}$$

The differential equation for seepage in the matrix system is factorless as:

$$(1-\omega)\frac{\partial p_{mD}}{\partial t_D} + \lambda\left(p_{mD} - p_{fD}\right) = 0 \tag{89}$$

The initial conditions of this low permeability reservoir are:

$$p_f = p_m = p_i (t = 0) \tag{90}$$

Assuming that the well produces at a constant rate q_{sc}, the inner boundary condition is:

$$r\left(\frac{\partial p_f}{\partial r} - G\right) = \frac{q_{sc}\mu}{2\pi k_{fi} h} \tag{91}$$

The inner boundary conditions are obtained without factorization:

$$r_D\left(\frac{\partial p_{fD}}{\partial r_D} - G_D\right)\Bigg|_{r=r_w} = -1 \tag{92}$$

Horizontal well fracture line source pressure is certain, then the inner boundary condition is:

$$p_f\big|_{r=0} = p_{wf} \tag{93}$$

The inner boundary conditions are obtained without factorization:

$$p_{fD}\big|_{r=0} = 0 \tag{94}$$

The mathematical model of unsteady seepage flow in low permeability reservoirs with dual media can be obtained from the coupled equations as:

$$\begin{cases} \dfrac{\partial^2 p_f}{\partial r^2} + \dfrac{1}{r}\dfrac{\partial p_f}{\partial r} - \dfrac{1}{r}G + \dfrac{\alpha k_m}{k_f}\left(p_m - p_f\right) = 0 \\ \phi_m C_m \dfrac{\partial p_m}{\partial t} + \dfrac{\alpha k_m}{\mu_o}\left(p_m - p_f\right) = 0 \\ r\left(\dfrac{\partial p_f}{\partial r} - G\right) = \dfrac{q_{sc}\mu}{2\pi k_{fi} h} \\ p_f = p_m = p_i (t = 0) \\ p_f\big|_{r=r_w} = p_{wf} \end{cases} \tag{95}$$

The mathematical model of unfactorized seepage is:

$$\begin{cases} \frac{\partial^2 p_{fD}}{\partial r_D^2} + \frac{1}{r_D}\frac{\partial p_{fD}}{\partial r_D} - \frac{G_D}{r_D} - \lambda k_m \left(p_{mD} - p_{fD}\right) = \omega \frac{\partial p_{fD}}{\partial t_D} \\ (1-\omega)\frac{\partial p_{mD}}{\partial t_D} + \lambda\left(p_{mD} - p_{fD}\right) = 0 \\ r_D\left(\frac{\partial p_{fD}}{\partial r_D} - G_D\right)\Big|_{r=r_w} = -1 \\ p_{fD}\big|_{r=r_w} = 0 \end{cases} \tag{96}$$

The mathematical model of seepage in a natural fracture system is obtained by biasing it:

$$\frac{\partial}{\partial t}\left(\frac{\partial p_{fD}^2}{\partial r_D^2} + \frac{1}{r_D}\frac{\partial p_{fD}}{\partial r_D} + \frac{G_D}{r_D}\right) - \lambda k_m \left(\frac{\partial p_{mD}}{\partial t} - \frac{\partial p_{fD}}{\partial t}\right) = \omega \frac{\partial^2 p_{fD}}{\partial t_D^2} \tag{97}$$

Available:

$$\frac{\partial p_{mD}}{\partial t} = \frac{\partial p_{fD}}{\partial t} - \frac{\omega}{\lambda k_m}\frac{\partial^2 p_{fD}}{\partial t_D^2} + \frac{1}{\lambda k_m}\frac{\partial}{\partial t}\left(\frac{\partial p_{fD}^2}{\partial r_D^2} + \frac{1}{r_D}\frac{\partial p_{fD}}{\partial r_D} - \frac{G_D}{r_D}\right) \tag{98}$$

$$\lambda\left(p_{mD} - p_{fD}\right) = \frac{1}{k_m}\left(\frac{\partial^2 p_{fD}}{\partial r_D^2} + \frac{1}{r_D}\frac{\partial p_{fD}}{\partial r_D} - \frac{G_D}{r_D} - \omega\frac{\partial p_{fD}}{\partial t_D}\right) \tag{99}$$

Substituting into the mathematical model of seepage in the matrix system and organizing the simplification yields:

$$\begin{gathered} \left(1-\omega-\frac{\omega}{k_m}\right)\frac{\partial p_{fD}}{\partial t_D} = \frac{1-\omega}{\lambda k_m}\frac{\partial}{\partial t}\left(\frac{\partial p_{fD}^2}{\partial r_D^2} + \frac{1}{r_D}\frac{\partial p_{fD}}{\partial r_D} - \frac{G_D}{r_D}\right) \\ -\frac{\omega}{k_m}\frac{\partial p_{fD}}{\partial t_D} + \frac{1}{k_m}\frac{\partial^2 p_{fD}}{\partial r_D^2} + \frac{1}{k_m r_D}\frac{\partial p_{fD}}{\partial r_D} - \frac{1}{k_m}\frac{G_D}{r_D} \end{gathered} \tag{100}$$

Laplace transform the above model such that:

$$\eta(r,s) = \int_0^\infty e^{-s\tau} p_{fD}(r,\tau)\,d\tau \tag{101}$$

The quadratic partial derivative term is after a Lattice transform as:

$$\int_0^\infty e^{-st}\frac{\partial^2 p_{fD}}{\partial r_D^2}dt = \frac{\partial^2 \int_0^\infty e^{-st} p_{fD}(r,t)}{\partial {r_D}^2} = \frac{d^2\eta_{fD}(r,s)}{dr^2} \tag{102}$$

The primary partial derivative term is after a Lattice transform as:

$$\int_0^\infty e^{-st}\frac{\partial p_{fD}}{\partial r_D}dt = \frac{\partial \int_0^\infty e^{-st} p_{\rho D}(r,t)}{\partial r_D} = \frac{d\eta_{fD}(r,s)}{dr} \tag{103}$$

with the time-independent term and the constant term are after a pull-apart transformation:

$$\int_0^{\infty} e^{-st}\left[\frac{1}{k_m}\frac{\partial^2 p_{fD}}{\partial r_D{}^2}+\frac{1}{k_m r_D}\frac{\partial p_{fD}}{\partial r_D}-\frac{1}{k_m}\frac{G_D}{r_D}\right]$$
$$dt=\frac{s}{k_m}\frac{\partial^2\eta_{fD}}{\partial r_D{}^2}+\frac{s}{k_m r_D}\frac{\partial\eta_{fD}}{\partial r_D}-\frac{s}{k_m}\frac{G_D}{r_D} \tag{104}$$

The left end term of the equal sign is after a pull-apart transformation:

$$\int_0^{\infty} e^{-st}\frac{\partial p_{fD}}{\partial t_D}dt=L\left(\frac{\partial p_{fD}}{\partial t}\right)=s\eta_{fD}(r,s) \tag{105}$$

The boundary conditions are transformed by a pull-apart transformation as:

$$r_D\left(\frac{\partial\eta_{fD}}{\partial r_D}+\frac{G_D}{s}\right)\Bigg|_{r=r_D}=-\frac{1}{s} \tag{106}$$

$$\eta_{fD}\big|_{r=r_D}=0 \tag{107}$$

The unsteady seepage model of a dual-media low-permeability reservoir in pull-out space can be obtained by associating the above equation as:

$$\begin{cases}\dfrac{\partial^2\eta_{fD}}{\partial r_D^2}+\dfrac{1}{r_D}\dfrac{\partial\eta_{fD}}{\partial r_D}-sD\eta_{fD}=-\dfrac{G_D}{sr_D}\\ r_D\left(\dfrac{\partial\eta_{fD}}{\partial r_D}+\dfrac{G_D}{s}\right)\Bigg|_{r=r_D}=-\dfrac{1}{s}\\ \eta_{fD}\big|_{r=r_D}=0\end{cases} \tag{108}$$

where: $D=\dfrac{\lambda+\omega(1-\omega)s}{\lambda+(1-\omega)s}$

r_D - the factorless distance of any point of the formation from the line sink, dimensionless;
r_{wD} - causeless radius of the horizontal well, dimensionless;
η_{fD} - the factorless pressure in pull-off space, dimensionless;
s - pull-type variable, dimensionless.

The mathematical model of seepage in the above equation belongs to the non-chiral second-order linear ordinary differential equation, and the corresponding chiral linear equation is:

$$\frac{\partial^2\eta_{fD}}{\partial r_D{}^2}+\frac{1}{r_D}\frac{\partial\eta_{fD}}{\partial r_D}-sD\eta_{fD}=0 \tag{109}$$

The above equation is the Bessel equation with zero-order imaginary bulk and the generalized solution is expressed as:

$$\eta_{fD1}=AK_0\left(\sqrt{sD}r_D\right)+BI_0\left(\sqrt{sDr_D}\right) \tag{110}$$

Eq:
$I_0(x)$ - Zero order first class modified Bessel function;
$K_0(x)$ - Zero-order second class modified Bessel function.

The solution of the non-chiral second-order linear equation using the basic methods of mathematics is given by:

$$\eta_{fD2} = \frac{G_D}{s} K_0\left(\sqrt{sD}r_D\right)\int_0^{r_D} I_0(\sqrt{sD}\tau)d\tau + \frac{G_D}{s} I_0\left(\sqrt{sD}r_D\right)\int_{r_D}^{\infty} K_0(\sqrt{sD}\tau)d\tau \tag{111}$$

Therefore, the solution of this mathematical model of seepage is:

$$\eta_{fD} = AK_0\left(\sqrt{sD}r_D\right) + BI_0\left(\sqrt{sD}r_D\right) + \frac{G_D}{s} K_0\left(\sqrt{sD}r_D\right) \int_0^{r_0} I_0(\sqrt{sD}\tau)d\tau + \frac{G_D}{s} I_0\left(\sqrt{sD}r_D\right)\int_{r_0}^{\infty} K_0(\sqrt{sD}\tau)d\tau \tag{112}$$

A partial derivation of the above equation is obtained:

$$\frac{\partial \eta_{fD}}{\partial r_D} = \frac{G_D}{s}\left[-\sqrt{sD}K_1\left(\sqrt{sD}r_D\right)\int_0^{r_D} I_0(\sqrt{sD}\tau)d\tau + \sqrt{sD}I_0\left(\sqrt{sD}r_D\right)\int_{r_0}^{\infty} K_0(\sqrt{sD}\tau)d\tau\right] - A\sqrt{sD}K_1\left(\sqrt{sD}r_D\right) + B\sqrt{sD}I_1\left(\sqrt{sD}r_D\right) \tag{113}$$

It follows from the Bessel function properties:

$$xK_1(x)\big|_{x\to 0} = 1 \tag{114}$$

$$I_1(x)\big|_{x\to 0} = 0 \tag{115}$$

Therefore, it is known that when $r_D \to 0$, then:

$$r_D\left(\frac{\partial \eta_{fD}}{\partial r_D} + \frac{G_D}{s}\right)\Bigg|_{r\to 0} = -A \tag{116}$$

Available:

$$A = \frac{1}{s} \tag{117}$$

Substituting into the equations in conjunction with the internal boundary conditions shows that:

$$B = \frac{-K_0\left(\sqrt{sD}r_{eD}\right) - G_D\begin{bmatrix} K_0\left(\sqrt{sD}r_D\right)\int_0^{r_{wD}} I_0(\sqrt{sD}\tau)d\tau \\ +I_0\left(\sqrt{sD}r_D\right)\int_{r_{wD}}^{\infty} K_0(\sqrt{sD}\tau)d\tau \end{bmatrix}}{sI_0\left(\sqrt{sD}r_{eD}\right)} \tag{118}$$

Define the new Green's function according to the source function as:

$$H\left(r_D\right) = sAK_0\left(\sqrt{sD}r_D\right) + sBI_0\left(\sqrt{sD}r_D\right) + G_D K_0\left(\sqrt{sD}r_D\right) \int_0^{r_0} I_0(\sqrt{sD}\tau)d\tau + G_D I_0\left(\sqrt{sD}r_D\right)\int_{r_0}^{\infty} K_0(\sqrt{sD}\tau)d\tau \tag{119}$$

Among them:

$$\begin{cases} A = \dfrac{1}{s} \\ B = \dfrac{-K_0\left(\sqrt{sD}r_{wD}\right) - G_D \begin{bmatrix} K_0\left(\sqrt{sD}r_{wD}\right)\int_0^{r_{wD}} I_0(\sqrt{sD}\tau)d\tau \\ +I_0\left(\sqrt{sD}r_{wD}\right)\int_{r_{wD}}^{\infty} K_0(\sqrt{sD}\tau)d\tau \end{bmatrix}}{sI_0\left(\sqrt{sD}r_{wD}\right)} \end{cases} \tag{120}$$

Applying the principle of pressure drop superposition, the pressure distribution of the continuous line source S can be obtained as:

$$\eta_{fijD} = \int_S q_{fijD} H\left(r_D\right) dS \tag{121}$$

3.2.2. Mathematical modeling of hydraulic fracture. The horizontal well axis is oriented in x direction, the number of hydraulic fractures is M, the fractures are of equal length, and the angle between the i rd hydraulic fracture and the x-axis is α_i. Each fracture is divided into $2N$ parts, and each fracture microelement is an independent flow.

The coordinates of the midpoint of the j th line sink of the i th crack are:

$$\left(x_{ij}, y_{ij}\right) = \left(-\frac{2N-2j+1}{2N} x_{Di} \sin\alpha_i, y_{Di} + \frac{2N-2j+1}{2N} x_{Dk} \cos\alpha_i\right) \tag{122}$$

Assuming that each of the line sinks on the i st hydraulic fracture has an equal yield, it can be seen from the above equation that the pressure drop produced by any line sink on the hydraulic fracture at any point is:

$$\eta_{fijD} = q_{fijD} \int_{x_{tx,j}}^{x_{Di,j=1}} H\left(R_D\right)\left(\sqrt{1+ctg^2\left(\alpha_i\right)}\right) dx_{wDi} \tag{123}$$

In the formula:

$$R_D = \sqrt{\left(x_D - x_{wD}\right)^2 + \left(y_D - y_{wD}\right)^2} \tag{124}$$

The expression for the pressure drop at the location of the k st crack can be found as:

$$\eta_{wkD} = \sum_{i=1}^{M} \sum_{j=1}^{2N} \frac{q_{fiD} L_r}{2N} \int_{x_{Di,j}}^{x_{tx,j=1}} H\left(R_D\right)\left(\sqrt{1+ctg^2\left(\alpha_i\right)}\right) dx_{wDi} \tag{125}$$

x_{ij} - horizontal coordinates of the midpoint of the j rd confluence of the i nd crack;
y_{ij} - vertical coordinates of the midpoint of the j th line sink of the i th crack;
x_{ft} - length of the left flank of the hydraulic crack, m;
x_{fr} - length of the right flank of the hydraulic crack, m;
x_{Di} - Uncaused horizontal coordinates of any point on the i nd crack;
y_{Di} - uncaused vertical coordinates of any point on the i th crack;
x_{Dk} - Uncaused transverse coordinates of any point on the k th crack;
y_{Dk} - the uncaused vertical coordinate of any point on the k th crack;
x_D -- Factorless transverse coordinates of any point in the stratigraphy;
y_D -- Uncaused vertical coordinates of any point in the stratigraphy;
x_{wD} -- Horizontal wells have no factorized transverse coordinates;
y_{wD} -- Horizontal wells have no factorized vertical coordinates;
q_{fi} -- i st hydraulic fracture yield, m^3/s;
q_{fijD} -- line density factorless yield of the j th line sink on the i rd hydraulic fracture, dimensionless;
q_{fiD} -- causeless yield of the i th hydraulic fracture, dimensionless;

α_i -- angle of the i th fracture to the horizontal well;
α_k -- angle of the k th fracture to the horizontal well.

3.2.3. Seepage mathematical model solution. Horizontal wellbores do not generate pressure drops, then there is:

$$\eta_{w1D} = \eta_{w2D} = \cdots = \eta_{wMD} = \eta_{wD} \tag{126}$$

Calculating M crack yield gives:

$$\sum_{i=1}^{M} q_{jiD} = \frac{1}{s} \tag{127}$$

Joining the above equations, the system of equations is obtained as follows:

$$\begin{bmatrix} A_{1,1} & A_{1,2} & \cdots & A_{1,M} & -1 \\ A_{2,1} & A_{2,2} & \cdots & A_{2,M} & -1 \\ \cdots & \cdots & \cdots & \cdots & -1 \\ A_{M,1} & A_{M,2} & \cdots & A_{M,M} & -1 \\ 1 & 1 & \cdots & 1 & 0 \end{bmatrix} \begin{bmatrix} q_{f1D} \\ q_{f2D} \\ \cdots \\ q_{fMD} \\ \eta_{wD} \end{bmatrix} = \begin{bmatrix} 0 \\ 0 \\ \cdots \\ 0 \\ 1/s \end{bmatrix} \tag{128}$$

Among them: $A_{k,i} = \sum_{j=1}^{2N} \frac{L_r}{2N} \int_{x_{Dj}}^{x_{Dj+1}} H\left(R_D\right)\left(\sqrt{1+ctg^2\left(\alpha_i\right)}\right) dx_{wDi}$

$$R_D = \sqrt{\begin{aligned}&\left(x_{Dk}\sin\alpha_k - \frac{2N-2j+1}{2N}x_{Di}\sin\alpha_i\right)^2 \\ &+\left(y_{Dk} + x_{Dk}\sin\alpha_A - y_{Di} - \frac{2N-2j+1}{2N}x_{Di}\cos\alpha_i\right)^2\end{aligned}} \tag{129}$$

This is obtained by considering the uncaused wellbore storage factor C_{wD} and the total skin factor s_c:

$$\eta_{wHD} = \frac{s\eta_{wD} + s_c}{s + s^2 C_{wD}\left(s\eta_{wD} + s_e\right)} \tag{130}$$

C_{wD} - Factorless wellbore storage coefficient, dimensionless:
s_c - skin coefficient, dimensionless.

Solving the above system of equations yields the pressure distribution of fractured horizontal wells in Laplace space, which can be converted to real space by numerical inversion methods. In this paper, the Stehfest numerical [31] inversion is utilized for the solution.

Assuming that the Laplace transform of $f(t)$ is $\overline{f}(s)$, the defining equation is:

$$\overline{f}(s) = L[f(t)] = \int_0^\infty f(t)e^{-st}dt \tag{131}$$

where the value of $f(t)$ in $t = T$ is calculated as:

$$f(T) = \frac{\ln 2}{T}\sum_{i=1}^{n} V_{i_s}\overline{f}\left(\frac{\ln 2}{T}i_s\right) \tag{132}$$

$$V_{i_s} = (-1)^{n/2+i_s} \sum_{k_s=\frac{i+1}{2}}^{\min(i_s,n/2)} \frac{k_s^{n/2}\left(2k_s\right)!}{\left(n/2-k_s\right)!k_s!\left(k_s-1\right)!\left(i_s-k_s\right)!\left(2k_s-i_s\right)!} \tag{133}$$

At this point, a semi-analytical solution for unstable seepage in fractured horizontal wells can be found by solving the above system of equations.

3.3. *Modeling of seepage in fractured inhomogeneous composite reservoirs*

The effect of natural fracture parameters on production capacity was investigated using fracture parameters and reservoir parameters of the Zhuang9 well area. The reservoir parameters and fracture parameters of Zhuang9 well area are shown in Table 1.

Table 1. Reservoir parameters and fracture parameters

Reservoir parameter	Parameter value	Reservoir parameter	Parameter value
Reservoir permeability($\times 10^{-3}\mu m^2$)	0.5	Oil volume coefficient(m^3/m^3)	1.35
Reservoir thickness(m)	14.7	Ground crude oil density (g/cm^3)	0.9256
Oil viscosity (mPa·s)	0.9941	Well radius (m)	0.15
Natural fracture length(m)	0.4—9.5	Boundary pressure (MPa)	16
Natural fracture opening (μm)	10—30	Bottom flow pressure (MPa)	7
Natural fracture line density (1/m)	1.8	For liquid radius (m)	150
Natural gap distance (m)	0.2—70		

3.3.1. Influence of Natural Fracture Parameters on Yield. Define the production increase as the percent increase in production with natural fractures relative to production without natural fractures. Figure 8 shows the effect of four lengths of cracks on production at different distances from the well when the crack opening is 20 μm and the number of cracks is 10. From the figure, it can be seen that the longer the natural cracks are, the greater the increase in production, and the maximum increase in production is about 65% without connecting to the well, and even if the cracks are only 0.4m long, the increase in production can reach nearly 30% without connecting to the well; the range of natural cracks that can play a role in increasing the production is within 9.5m from the well.

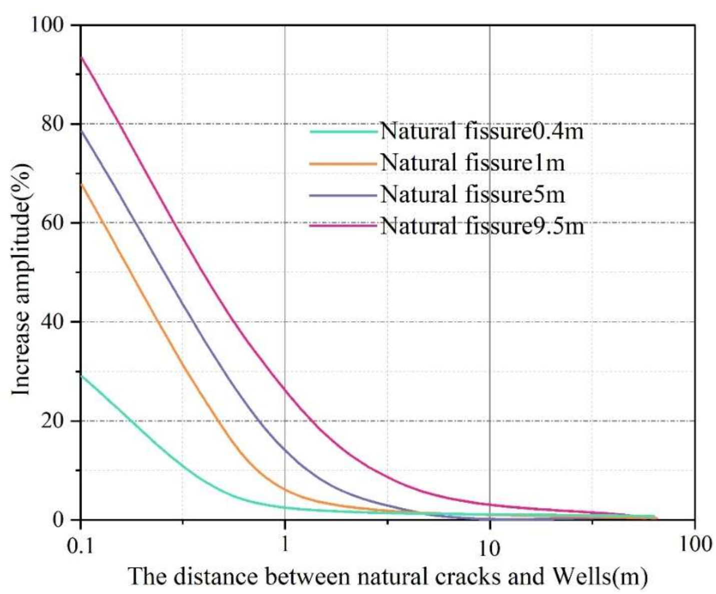

Fig. 8. The effect of fracture length on production

Figure 9 shows the effect of three kinds of fracture openings on the production at different distances from the well when the number of fractures is 10 and the length is 1m. Fracture openness has a large impact on the production, the larger the openness, the larger the increase in production, but the increase in production is not proportional to the natural fracture openness, and the increase in production is getting smaller and smaller with the increase in openness. The main reason is that the relationship between the permeability of natural cracks and the degree of opening is quadratic, with the increase of crack opening, the permeability of cracks increases greatly, and the seepage resistance in the crack development area decreases greatly, but the ability of the outer boundary to supply fluids is limited, so the yield increase will slow down after a certain magnitude.

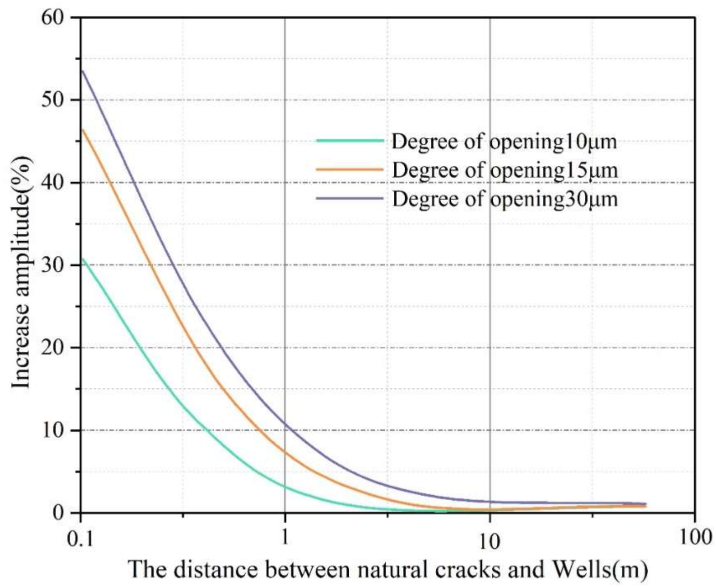

Fig. 9. The effect of crack opening on yield

Figure 10 shows the effect of four numbers of cracks at different distances from the well on the production at a crack opening of 20 μm and a length of 1m. As can be seen from the figure, the production increases rapidly with increasing number of cracks, but the increase is getting smaller and smaller, and the difference in production increase between 10 cracks and 40 or 60 cracks is only about 10%.

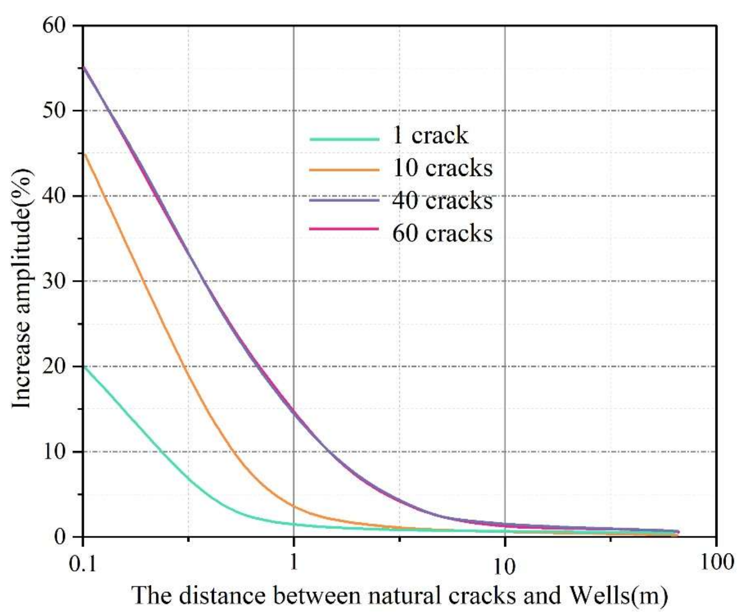

Fig. 10. The effect of the fracture quantity on production

Figure 11 shows the effect of four line densities of cracks at different distances from the well on the production at a crack opening of 20 μm and a length of 1 m. The effect of the cracks on the production at different distances from the well is shown in Fig. 11. As can be seen from the figure, the production increase of the fractures increases with the increase of line density. After the range of 9.5m from the well, the production increase of the cracks is basically negligible, which is consistent with the pattern when the number of cracks is constant.

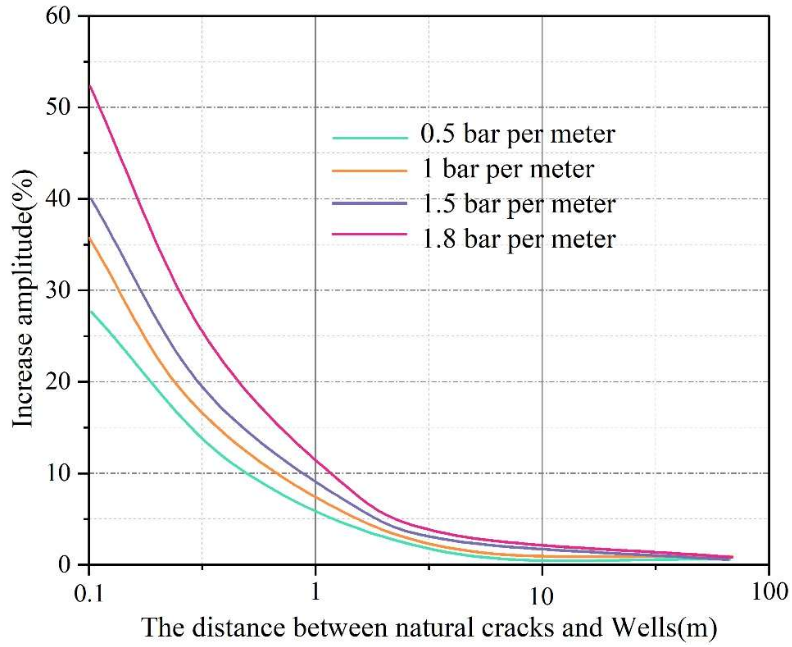

Fig. 11. The effect of fracture line density on production

3.3.2. Effect of natural fracture parameters on pressure distribution. The effect of natural seam parameters on pressure at fracture line density: 1.5 lines/m, openness: 20 μm, and length: 1 m is shown in Fig. 12. When there is no natural fracture, the pressure curve is the steepest and the pressure drop is the largest within 9m from the well in the reservoir. When a natural fracture exists, the pressure curve is more gentle and the pressure drop is smaller at the place where the natural fracture develops; the closer the fracture is to the well, the larger the pressure drop is in the reservoir and the larger the production is. According to the pressure curve, the main reason for the large increase in production of the natural fracture shown in the previous yield curve within 9m from the well is that the small seepage area around the well leads to a large pressure gradient and high seepage resistance, and the natural fracture has a large capacity of conduction, which improves the seepage capacity of the reservoir around the well, so the increase in production is larger; whereas, in the reservoir farther away from the well, the area of fluid seepage is large, the pressure gradient is small, and the seepage velocity of the fluid is In the reservoir farther away from the well, the fluid seepage area is large, the pressure gradient is small, the fluid seepage velocity is low, and the seepage resistance is relatively small, so the role played by the natural fracture becomes smaller, and the production increase is small.

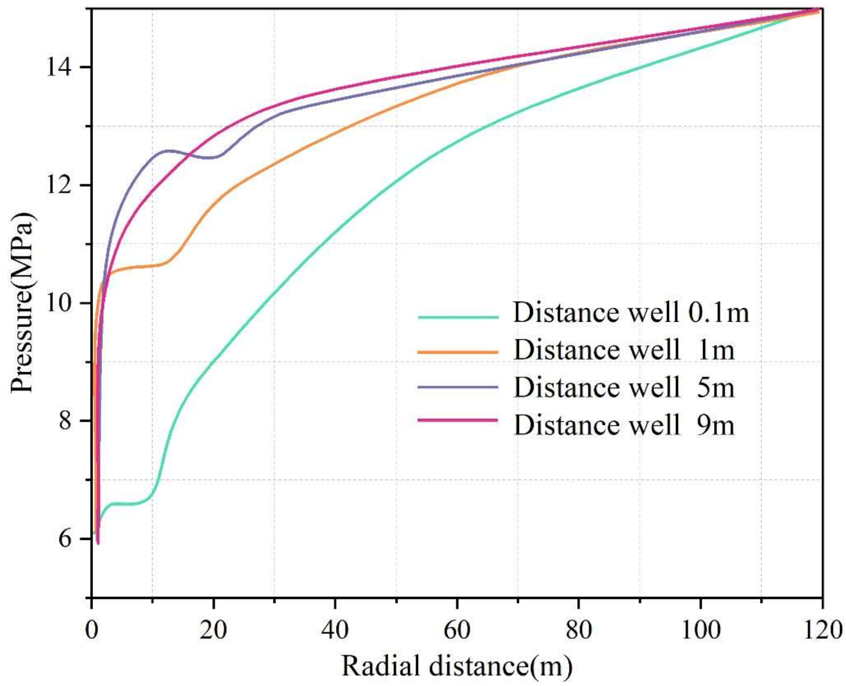

Fig. 12. The effect of natural seam parameters on stress

3.4. Optimization of fracture parameters for repeated modification of volumetric fracturing

Based on the repetitive fracturing fluid-solid coupling model, Well 1, Well 2, and Well 3 are taken as the research objects, and the orthogonal experimental design method is used for the optimization of repetitive modification fracture parameters in volumetric fracturing. Orthogonal test design is a multifactor and multilevel test design method, which can achieve results equivalent to a large number of full-scale tests with a minimum number of tests. The levels of each factor in the orthogonal test for the study wells are shown in Table 2. The fracture parameters in this study include: primary fracture half-length, fracture network bandwidth, primary fracture conductivity, and secondary fracture conductivity. Sixteen sets of scenarios were established for each of the study wells WELL 1, WELL 2, and WELL 3, and volumetric repeat fracturing was simulated at the optimal repeat fracturing timing for each well, and the magnitude of the influence of each factor on the repeat fracturing production increase potential of each well was determined by analyzing the difference in the percentage of cumulative oil increase in the wells corresponding to the repeat fracturing at 90% of the wells' water content after the repeat fracturing under the various scenarios.

Table 2. Study well orthogonal test factors

Factor	The main crack is half long(m)	Network bandwidth(m)	Main fracture guide capacity ($10^{-3}\mu m^2\cdot m$)	Subfracture conductivity ($10^{-3}\mu m^2\cdot m$)
Level 1	10	10	10	15
Level 2	50	20	50	25
Level 3	100	40	100	35
Level 4	150	80	150	45

In this paper, the mean value of the percentage of accrued oil at different levels of re-pressurization is calculated for each factor, and the extreme difference of the percentage of accrued oil at different levels is solved on this basis. The extreme deviation of the percentage of cumulative oil gain from repeated fracturing at different levels for each factor in the study wells is shown in Table 3. The magnitude of the extreme deviation reflects the contribution of each seam network factor to the cumulative oil increase percentage of repeat fracturing. The larger the extreme difference, the greater the influence of the factor on the repeat fracturing effect, and the smaller the extreme difference, the smaller the influence of the factor on the repeat fracturing effect of the well. The results show that the extreme difference of repeated fracturing cumulative oil increase percentage for each fracture parameter in WELL 3 (23.25%) is larger than that in WELL 1 (8.25%) and WELL 2 (6.75%). The order of the influence of factors is: main fracture half-length > fracture network bandwidth > main fracture inflow capacity > secondary fracture inflow capacity; WELL 1 is located in the high permeability zone, and the fracture network bandwidth has the greatest influence on the cumulative percentage of oil added by repeated fracturing after turning to fracture, and the order of the influence of factors is: fracture network bandwidth > main fracture half-length > main fracture inflow capacity > secondary fracture inflow capacity; WELL 2 is located in the low-permeability zone. The Well 2 well is in low permeability area, and the influence of slit network bandwidth and main fracture inflow capacity on the cumulative percentage of oil gain from repeated fracturing is large, and the order of influence of the factors is: slit network bandwidth>main fracture inflow capacity>main fracture half-length>subfracture inflow capacity.

Table 3. The factors of the various factors were compared under different levels

Well name	The main crack is half long(m)	Network bandwidth(m)	Main fracture guide capacity ($10^{-3}\mu m^2 \cdot m$)	Subfracture conductivity ($10^{-3}\mu m^2 \cdot m$)
Well 1	8.25	14.75	6.75	3.5
Well 2	6.75	9.75	8.75	2.75
Well 3	23.25	17.75	7.25	5

The extreme difference of the repeat fracturing cumulative oil percentage for each parameter is shown in Table 4. It is found that different repetitive fracturing main fracture half-lengths and cumulative oil increment percentages of the wells: WELL 3 repetitive fracturing cumulative oil increment percentage increases and then decreases with the increase of the main fracture half-length, and when the length of the repetitive fracture is more than 100 m, the repetitive fracture communicates with the hydraulic drive leading edge of the left injection well, and the water content rises faster, and the effect of repetitive fracturing becomes poorer; WELL 1 and WELL 2 repetitive fracture communicates with the area of residual oil richness and the repetitive fracturing WELL 1 and WELL 2 repressurization shifts the fracture to communicate the remaining oil-rich area, and the effect of repressurization becomes better with the increase of the half-length of the main fracture; the optimal repressurization half-length of the main fracture for WELL 1 and WELL 2 is 150m, and the optimal repressurization half-length for WELL 3 is 100m.

In the main fracture inflow capacity, the repressurized cumulative oil percentage of each studied well increases with the increase of main fracture inflow capacity, and the main fracture inflow capacity has a greater impact on WELL 2, which is located in a low-permeability zone, so the focus of volumetric repetitive fracturing should be on improving the fracture inflow capacity of the sidetracks located in low-permeability zones; the optimal repressurized main fracture inflow capacity of WELL 3, WELL 2, and WELL 1 is $150\times10^{-3}\mu m^2 \cdot m$.

In the case of the slit network bandwidth and cumulative oil increase percentage, the cumulative oil increase percentage of repressurization of each well increases and then decreases with the increase of slit network bandwidth. When the slit network bandwidth is small, with the increase of slit network bandwidth, the reservoir reforming area increases, the pressure inside the slit network system is easier to propagate, and it is easier for the crude oil to flow from matrix to fracture, which makes the repressurization effect become better, and when the slit network bandwidth is large, the wells have faster increase of water content and lower oil production rate. Comparing Well 1 and Well 2, it is found that the lower the reservoir permeability, the larger the optimal repressurization fracture network bandwidth is; the optimal repressurization fracture network bandwidth of Well 3 and Well 1 is 20 m, and the optimal repressurization fracture network bandwidth of Well 2 is 40 m.

In the subfracture inflow capacity and cumulative oil increase percentage, the cumulative oil increase percentage of repetitive fracturing increases slowly with the increase of repetitive fracturing subfracture inflow capacity in each study well, and the subfracture inflow capacity has a small effect on the oil increase effect of repetitive fracturing; the optimal subfracture inflow capacity of WELL 1, WELL 2, and WELL 3 is $45\times10^{-3}\mu m^2\cdot m$.

Table 4. The total amount of repeated fracturing of each parameter is the worst

Optimization parameter	Parameter value	The percentage of repressing oil(%)		
		Well 1	Well 2	Well 3
Main fissure(m)	10	62.49	54.35	79.85
	50	66.92	56.15	93.39
	100	69.32	57.34	105.25
	150	71.24	62.86	100.34
Main fracture guide ability($10^{-3}\mu m^2\cdot m$)	10	64.17	54.11	89.79
	50	69.44	56.51	94.10
	100	73.40	59.38	95.43
	150	73.75	65.97	99.37
Seam bandwidth(m)	10	63.46	53.76	83.57
	20	73.04	58.19	98.42
	40	71.00	59.86	84.17
	80	49.09	50.65	80.82
Subfracture conductivity ($10^{-3}\mu m^2\cdot m$)	15	65.14	61.30	91.35
	25	68.13	62.37	92.68
	35	69.20	64.77	95.55
	45	70.41	65.62	97.83

4. Conclusion

In this paper, using the finite element model, combined with the seepage characteristics of low-permeability reservoirs, we constructed a mathematical model of unstable seepage in fractured horizontal wells based on the oil seepage field pressure distribution mode, and analyzed the change of fractured horizontal well production over time under different mobilization radius conditions.

1) Stress-strain, porosity and permeability in low-permeability reservoirs are functions of time and space. Spatially, in the region near the bottom of the well, these parameters are more variable; while the farther away from the bottom of the well region, the less they are affected. Temporally, the stress-strain, porosity, and permeability change more for the early stages of production in a closed reservoir.

2) Simulation of the distribution of pressure in fractured horizontal wells found that among several parameters, the relative position of the fracture to the well has a large impact on production, and this parameter is also a parameter that can be adjusted by human beings. For fractured reservoirs, it is of great significance to consider the relative position of the fracture to the well when laying out the well.

3) Through the analysis of the extreme difference of the cumulative oil increase percentage of repeated fracturing, it is determined that the order of the influence of each factor on the side wells in the high permeability strip is as follows: the width of the slit network > the half-length of the main fracture > the main fracture inflow capacity > the secondary fracture inflow capacity, and the order of the influence of each factor on the corner wells is as follows: the half-length of the main fracture > the bandwidth of the slit network > the main fracture inflow capacity > the secondary fracture inflow

capacity, and the order of the influence of each factor on the side wells in low permeability zones is as follows: the half-length of the main fracture > the bandwidth of the main network > the main fracture inflow capacity > the secondary fracture inflow capacity. The order of the influence of each factor for the side wells in the low-permeability zone is: main fracture flow-conducting capacity>seam network bandwidth>main fracture half-length>secondary fracture flow-conducting capacity, and the optimal values of the influencing factors for each study well are determined.

References

[1] Ji, B., & Fang, J. (2023). An overview of efficient development practices at low permeability sandstone reservoirs in China. Energy Geoscience, 4(3), 100179.

[2] Wenrui, H. U., Yi, W. E. I., & Jingwei, B. A. O. (2018). Development of the theory and technology for low permeability reservoirs in China. Petroleum Exploration and Development, 45(4), 685-697.

[3] Kang, W. L., Zhou, B. B., Issakhov, M., & Gabdullin, M. (2022). Advances in enhanced oil recovery technologies for low permeability reservoirs. Petroleum Science, 19(4), 1622-1640.

[4] Wu, Y., Huang, Z., Zhao, K., Zeng, W., Gu, Q., & Zhang, R. (2020). Unsteady seepage solutions for hydraulic fracturing around vertical wellbores in hydrocarbon reservoirs. International Journal of Hydrogen Energy, 45(16), 9496-9503.

[5] Lufeng, Z., Fujian, Z., Shicheng, Z., Jin, W., & Yuechun, W. (2019). Evaluation of permeability damage caused by drilling and fracturing fluids in tight low permeability sandstone reservoirs. Journal of Petroleum Science and Engineering, 175, 1122-1135.

[6] Zhang, L., Li, Z., Lai, F., Li, H., Adenutsi, C. D., Wang, K., ... & Xu, W. (2019). Integrated optimization design for horizontal well placement and fracturing in tight oil reservoirs. Journal of Petroleum Science and Engineering, 178, 82-96.

[7] Zhao, X., Li, M., Yan, K., & Yin, L. (2023). Revolutionizing Tight Reservoir Production: A Novel Dual-Medium Unsteady Seepage Model for Optimizing Volumetrically Fractured Horizontal Wells. Energy Engineering, 120(12).

[8] Li, M., Yi, X., & Li, C. (2021). Seepage model for multiple-fractured horizontal wells in coal bed methane reservoirs. Energy Sources, Part A: Recovery, Utilization, and Environmental Effects, 43(4), 506-515.

[9] Li, J., Zhou, X., Liu, X., Gayubov, A., & Shamil, S. (2023). Cross-scale seepage characteristics of fractured horizontal wells in tight gas reservoirs. ACS omega, 8(27), 24291-24301.

[10] Zhou, J., He, S., Tang, M., Huang, Z., Chen, Y., Chi, J., ... & Yuan, P. (2018). Analysis of wellbore stability considering the effects of bedding planes and anisotropic seepage during drilling horizontal wells in the laminated formation. Journal of Petroleum Science and Engineering, 170, 507-524.

[11] Li, Y., Cheng, Y., Yan, C., Song, L., Liu, H., Tian, W., & Ren, X. (2020). Mechanical study on the wellbore stability of horizontal wells in natural gas hydrate reservoirs. Journal of Natural Gas Science and Engineering, 79, 103359.

[12] He, J., Li, G., & Yu, L. (2021, February). Analysis of Seepage Law of Precipitation in Horizontal Wells with Low Permeability Formation. In IOP Conference Series: Earth and Environmental Science (Vol. 668, No. 1, p. 012075). IOP Publishing.

[13] Wu, M., Zhu, J., Li, L., & Li, P. (2020). Calculation of perforated vertical and horizontal well productivity in low-permeability reservoirs. SPE Drilling & Completion, 35(02), 218-236.

[14] Tang, M., Zhang, G., He, S., Kong, L., Deng, F., & Lei, H. (2023). Analysis of seepage and temperature fields and their influence on collapse pressure while drilling in shale oil reservoirs. Geoenergy Science and

Engineering, 231, 212410.

[15] Ren, Z., Qu, Z., Jia, S., Zhang, G., Fan, C., Feng, T., & Ren, Z. (2023). Study on seepage model of Multiple Horizontal wells with complex fracture networks in tight Reservoir Based on boundary element method. Natural Gas Industry B, 10(3), 254-269.

[16] Yang, Y., Xiong, W., Liao, G., Gao, S., Shen, R., Zhang, J., & Li, Q. (2022). Flow mechanism of production decline during natural depletion after hydraulic fracturing of horizontal wells in tight oil reservoirs. Petroleum Science and Technology, 40(4), 383-400.

[17] Wei, B., Nie, X., Zhang, Z., Ding, J., Shayireatehan, R., Ning, P., ... & Xiong, J. (2023). Zoning Productivity Calculation Method of Fractured Horizontal Wells in High-Water-Cut Tight Sandstone Gas Reservoirs under Complex Seepage Conditions. Processes, 11(12), 3308.

[18] Jiang, R., Zhang, C., Cui, Y., Wang, Q., Zhang, W., & Zhang, F. (2019). Characteristics of transient pressure performance of horizontal wells in fractured-vuggy tight fractal reservoirs considering nonlinear seepage. Oil & Gas Science and Technology–Revue d'IFP Energies nouvelles, 74, 57.

[19] Ce, W., Shanbin, H., Mingyu, W., & Fafeng, X. (2022). Density cutting volume fracturing technology for horizontal wells in the ultra-low permeability reservoirs: A case study of the Yuan284 area in the Huaqing oilfield Ordos Basin, China. Arabian Journal of Geosciences, 15(16), 1409.

[20] Zhou, C. B., Chen, Y. F., Hu, R., & Yang, Z. (2023). Groundwater flow through fractured rocks and seepage control in geotechnical engineering: Theories and practices. Journal of Rock Mechanics and Geotechnical Engineering, 15(1), 1-36.

[21] Gao, S., Yang, Y., Liao, G., Xiong, W., Liu, H., Shen, R., ... & An, W. (2022). Experimental research on inter-fracture asynchronous injection-production cycle for a horizontal well in a tight oil reservoir. Journal of Petroleum Science and Engineering, 208, 109647.

[22] He, S., Wang, W., Tang, M., Hu, B., & Xue, W. (2014). Effects of fluid seepage on wellbore stability of horizontal wells drilled underbalanced. Journal of Natural Gas Science and Engineering, 21, 338-347.

[23] He, S., Zhou, J., Chen, Y., Li, X., & Tang, M. (2017). Research on wellbore stress in under-balanced drilling horizontal wells considering anisotropic seepage and thermal effects. Journal of Natural Gas Science and Engineering, 45, 338-357.

[24] Liu, P., Wang, Q., Luo, Y., He, Z., & Luo, W. (2021). Study on a new transient productivity model of horizontal well coupled with seepage and wellbore flow. Processes, 9(12), 2257.

[25] Zhao, Y., Zhang, L., Xiong, Y., Zhou, Y., Liu, Q., & Chen, D. (2016). Pressure response and production performance for multi-fractured horizontal wells with complex seepage mechanism in box-shaped shale gas reservoir. Journal of Natural Gas Science and Engineering, 32, 66-80.

[26] He, J., Niu, X., Meng, Q., Guo, F., Wang, H., Liu, Y., ... & Zhu, Y. (2023). Analysis of seepage mechanism and productivity model of multi-stage fractured horizontal well in tight sandstone gas reservoir. Petroleum Science and Technology, 41(21), 2055-2070.

[27] Ke, W., Luo, W., Miao, S., Chen, W., & Hou, Y. (2023). A Transient Productivity Prediction Model for Horizontal Wells Coupled with Oil and Gas Two-Phase Seepage and Wellbore Flow. Processes, 11(7), 2012.

[28] Antonets V. A. & Antonets M. A.. (2023). Application of the Variational Principle to Create a Measurable Assessment of the Relevance of Objects Included in Training Databases. Optical Memory and Neural Networks(Suppl 2),S265-S269.

[29] Jiaxin Wang,Kun Wang,Zhen Guo Yan,Xiaofeng He & Tiegang Liu. (2025). GPGPU-based heterogeneous parallel implementation of direct discontinuous Galerkin methods. Mathematics and Computers in Simulation362-391.

[30] Álvarez Enrique,Murillo Ricardo & Plaza Ramón G.. (2022). Spectral instability of small-amplitude periodic waves for hyperbolic non-Fickian diffusion advection models with logistic source. Mathematical Modelling of Natural Phenomena

[31] Xiaoxu Dong,Shunchu Li,Zhibin Liu & Hehua Wang. (2021). Similar Constructing Method and Gaver-Stehfest Numerical Inversion Equation for Solving the Composite Reservoir Models Under Three Outer Boundary Conditions. Arabian Journal for Science and Engineering(9),1-15.